Substrates Induce Conformational Changes in Human Anion Exchanger 1 (hAE1) as Observed by Fluorescence Resonance Energy Transfer†

Prithwish Pal,*,‡ Dmitry Lebedev,§ Sara Salim, and Philip A. Knauf

Department of Biochemistry and Biophysics, University of Rochester, 601 Elmwood Avenue, Box 712, Rochester, New York 14642

Received September 20, 2005; Revised Manuscript Received January 29, 2006

ABSTRACT: The one-for-one exchange of Cl^- and HCO_3^- ions is catalyzed by human erythrocyte anion exchanger 1 (hAE1) through a ping-pong mechanism whereby the protein exists in two main conformations, with the single anion-binding site exposed at either the cytoplasmic (inner) side (E_i) or the extracellular side (E_o), with interconversion between the two states being possible only after anion binding. Steady-state and time-resolved resonance energy transfer (FRET) techniques were used to determine the distance of the binding site for diTBA (bis-(1,3-diethylthiobarbituric acid)trimethine oxonol), a high affinity fluorescent oxonol inhibitor of hAE1, from a benchmark site (probably Lys-430) labeled by external fluorescein maleimide (FM). Using red cell ghost membranes, energy transfer distances were measured in media containing different anions between FM as the donor, covalently attached to one monomer, and diTBA as the acceptor, reversibly bound to the adjacent monomer of a hAE1 dimer. Energy transfer increased significantly in chloride or bicarbonate buffers relative to conditions where no transportable anions were present, that is, in citrate buffer. These differences in transfer efficiencies were interpreted in light of the conformational distributions of hAE1 in various buffers and the possible effects of diTBA itself on the distribution. The analysis indicates that the diTBA binding site comes closer to the FM site by ∼7 Å in chloride buffer as compared to that in citrate (or equivalent changes in diTBA orientation occur) because of the effects of anion binding. This provides the first direct physical evidence for structural changes in hAE1 induced by substrates.

The human erythrocyte anion exchanger hAE1[1], a member of the SLC4 family of bicarbonate transporters, carries out the electroneutral exchange of chloride for bicarbonate ions across the red blood cell plasma membrane (*1*). The protein consists of two functionally and structurally different domains: (a) the *N*-terminal cytoplasmic domain (1−404) that acts as an anchorage point for the red cell cytoskeleton (*2*) and (b) the *C*-terminal membrane embedded domain (405−911) that is necessary as well as sufficient for anion exchange. Because of its high abundance in red blood cells (∼50% of the integral membrane proteins), the transport and biochemical properties of hAE1 have been characterized extensively. However, there is insufficient information to construct a structural model of the exchange mechanism. The cytoplasmic domain has been individually crystallized and its structure resolved to 2.6 Å resolution (*3*), but for the membrane domain, only a 20 Å resolution electron diffraction structure is available (*4*, *5*). Both of these structures as well as chromatographic (*6*), cross-linking (*7*, *8*), and energy transfer analyses (*9*) have revealed that under most conditions hAE1 exists as a dimer, although the monomer is probably the functional unit of the protein (*10*). The membrane domain of each monomer is thought to contain 12 to 14 transmembrane (TM) segments with a few extended loops at both the cytoplasmic and extracellular faces of the protein (*11*−*15*).

Data on the transport rates under a wide variety of conditions as well as data on the effects of inhibitors strongly indicate that hAE1 carries out anion exchange by a ping-pong mechanism (Figure 1), whereby the transporter has two conformational states: one with the anion binding site facing inside toward the cytoplasm (inward facing or E_i) and another with the binding site facing toward the outside (outward facing or E_o) (*16*−*19*). Substrate anions can bind only from the side toward which the binding side faces. Interconversion between the outward- and inward-facing states can take place only when an anion is bound, indicating that anion binding induces a conformational change that lowers the high free-energy barrier between the two forms. Thus, to understand the structural mechanism of hAE1 transport, two questions need to be answered: (a) What conformational changes occur upon anion binding? (b) What are the structural differences between the inward- and outward-facing forms of the protein? To answer these questions, effective tools are

† This work was supported by NIH (NIDDK) grant R01 DK27495.

* To whom correspondence should be addressed. Tel: 919-843-2752. Fax: 919-966-5640. Email: ppal@med.unc.edu.

‡ Present address: Department of Pharmacology, University of North Carolina, Chapel Hill, NC 27599.

§ Present address: St. Petersburg Nuclear Physics Institute, RAS Gatchina, Leningrad, District 188300, Russia.

[1] Abbreviations: hAE1, human anion exchanger 1; TM, transmembrane; FRET, fluorescence resonance energy transfer; DMSO, dimethyl sulfoxide; FM, fluorescein-5-maleimide; EM, Eosin-5-maleimide; RBC, red blood cells; diTBA, bis-(1,3-diethylthiobarbituric acid)trimethine oxonol; DIDS, 4, 4′-diisothiocyanato-stilbene-2,2′-disulfonate; SET, specific energy transfer; NSET, nonspecific energy transfer; WW781, [3-methyl-1-*p*-sulfophenyl-5-pyrazolone-(4)]-[1,3-dibutylbarbituric acid]-pentamethine oxonol; TCSPC, time-correlated single photon counting.

10.1021/bi051916r CCC: $33.50
Published on Web 04/27/2006

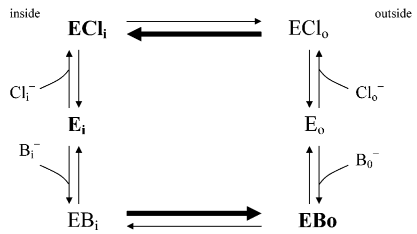

FIGURE 1: Ping-pong mechanism of anion transport. Bold type is used to represent the predominant forms of AE1: $E_i \gg E_o$, $ECl_i \gg ECl_o$ but $EB_i \ll EB_o$.

required to recruit the protein to its different conformational states.

The conformational distribution of hAE1 in the absence of any substrates is highly asymmetric. Both at 0 °C and at physiological temperatures, E_o/E_i (= A) ≤ 0.1; therefore, the inward-facing form, E_i, is highly favored (*19*). This appears to be true also when chloride is present as the substrate, with $^{35}Cl^-$ NMR data at 0 °C indicating that the chloride-loaded site asymmetry, ECl_o/ECl_i (A_{Cl}), is 0.14 (*20*, *21*). In recent experiments, the rate of heteroexchange of internal chloride, Cl_i, for external bicarbonate, B_o, at 0 °C was found to be much slower than the rate of heteroexchange of B_i for Cl_o (*22*, *23*). Calculations based on a ping-pong model for Cl/B heteroexchange that is consistent with the experimental data for Cl/Cl and B/B exchange indicate that the observed fluxes can be explained only if EB_o/EB_i (A_B) ≥ 10. Limited data at body temperature indicate similar asymmetry (*24*).

This means that far more bicarbonate-loaded sites face the outside than the inside. The opposite asymmetries in the presence of chloride or bicarbonate imply that it is possible to recruit hAE1 preferentially to its outward-facing (in bicarbonate) or inward-facing (in chloride or citrate, an anion with very low affinity for the substrate binding site) conformations by using the appropriate substrate. To determine if the binding of substrates or the substitution of one substrate for another does indeed alter hAE1 conformation, fluorescence resonance energy transfer (FRET) has been used as a tool to determine intermonomeric distances in hAE1 in the presence of different anions.

FRET has been widely used as a spectroscopic ruler for distance measurements in biological systems (*25*). Energy transfer can be quantified by measuring either the quenching of donor steady state fluorescence intensity or the decrease in the donor fluorescence lifetime. To measure conformational changes in hAE1, a benchmark site (probably Lys-430) was labeled externally with fluorescein maleimide (FM) to act as the energy transfer donor. Energy transfer was then measured between FM and a noncovalently bound fluorescent oxonol inhibitor of hAE1, diTBA, which binds to the adjacent monomer. Using both steady state and time-resolved methods, it is shown that the binding of substrate anions causes a shortening of the distance between these two sites, thus providing physical evidence for a conformational change in hAE1. Portions of this work have appeared previously in abstract form (*26*).

EXPERIMENTAL PROCEDURES

Cell Preparation. Blood drawn from apparently healthy donors with their written consent was supplemented with heparin and kept on ice. The blood samples were washed three times with 150KH (150 mM KCl, 24 mM HEPES, and 24 mM sucrose) at pH 6.9 at 0 °C. White blood cells were removed by aspiration. Red blood cells (RBCs) were made up to 50% hematocrit in 150KH for further experiments.

External Labeling with FM. RBCs were diluted to 5% hematocrit in 162KH (162 mM KCl, 20 mM HEPES, and 24 mM sucrose) at pH 8.0 and incubated at 37 °C for 30 min. The cells were then washed once with 162KH at pH 8.0 and then resuspended at 50% or 25% hematocrit. FM (Molecular Probes, Eugene, OR) was added from a 100mM stock in dimethyl sulfoxide (DMSO) to the cell suspension with gentle vortexing. The final concentration in the extracellular volume was 1.2 mM, and the suspension was incubated in the dark at 37 °C for 1 h, unless specified otherwise. The reaction was stopped by adding an ice-cold solution of 150KH at pH 6.9 containing 0.5% BSA, and the labled RBC's were washed three more times with 150KH and stored at 50% hematocrit in the same buffer. Control cells were treated in the same manner but without adding FM.

Measurement of Anion Exchange Activity. Anion exchange activity was determined by radioisotope measurements of $^{36}Cl^-$ self-exchange by the rapid filtration technique of Dalmark and Wieth (*27*). Briefly, labeled or unlabeled cells at 25% hematocrit in 150KH (pH 6.9) were incubated with $^{36}Cl^-$ for 10 min at room temperature and then on ice until use. After centrifugation to remove the supernatant, the cells were resuspended in 150KH (pH 6.9) at 0 °C and rapid samples were taken with syringe filters (*22*).

Preparation of RBC Ghosts, Stoichiometry, and Gel Electrophoresis. The cells were lysed in 5P(8) buffer (5mM Na_2PO_4 and 1mM EGTA at pH 8) containing freshly added 0.2 mM of the protease inhibitor, phenyl methyl sulfonyl fluoride (PMSF), at 0 °C for 5 min. They were centrifuged at 30 000*g*, and the supernatant and the sticky pellet were removed by aspiration. The ghosts were further washed four to six times in 5P(8) until the control ghosts (not labeled by FM) appeared white. The total protein concentration in the ghosts was determined with the BCA Protein Assay Kit (Pierce, Rockford, IL), and hAE1 was assumed to comprise 25% of the total membrane protein (*28*). FM concentration in labeled ghosts (FM-ghosts) was determined by solubilizing in 0.2% SDS and measuring the optical density at 492 nm (with solubilized control ghosts as blanks). An extinction coefficient of 55 000 $M^{-1}cm^{-1}$ was assumed for FM (*29*, *30*). For SDS−PAGE, ghost samples were solubilized in a Laemmli buffer (Biorad, Hercules, CA) and heated at 95 °C for 5 min before loading on a 12% polyacrylamide gel. The gels were subsequently analyzed by fluorescent imaging (FluorImager 575, excitation 480 nm and emission 530 nm), and FM labeling specificity was determined from the ratio of the fluorescence within the peak corresponding to hAE1 to the total fluorescence throughout the lane using ImageQuant software.

Steady State Fluorescence Measurements and FRET. Steady state fluorescence was measured on a modified Photon Technologies, Inc. (Monmouth Junction, NJ) Alphascan fluorimeter, using the Felix software provided by the manufacturer. The samples were contained in a 1 cm optical glass cuvette and were thoroughly mixed with a Teflon stirrer. Usually, an aliquot of the ghost suspension was added to a cuvette containing 1.9 mL of the relevant buffer and 0.1 mL of DMSO to give a final concentration of 20 nM hAE1. A final concentration of 50 nM bis-(1,3-diethylthiobarbituric acid)trimethine oxonol (diTBA) pre-mixed in 0.45 mL of buffer was added to the cuvette with vigorous stirring. After diTBA fluorescence reached a plateau, 4,4′-diisothiocyanato-stilbene-2,2′-disulfonate (DIDS) was added to a final concentration of 20 μM to remove the hAE1-bound diTBA. The diTBA saturation experiments were conducted in a similar manner, except that diTBA was added first followed by unlabeled ghosts, which were mixed by a pipet, and no DMSO was used (the effect of DMSO was found to be negligible). Excitation and emission slits were set to 3 nm in all cases. For the simultaneous detection of donor and acceptor fluorescence, the emission monochromator was set to flip between two wavelengths. All steady state spectra and time based intensity plots are shown with the corresponding buffer backgrounds subtracted. The various buffers used were the chloride buffer: 150 mM KCl and 20 mM HEPES at pH 8.0; bicarbonate buffer: 150 mM $KHCO_3$ and 20 mM HEPES at pH 8.0; and citrate buffer: 25 mM K-citrate and 20 mM HEPES at pH 8.0.

Specific and nonspecific energy transfer components were determined as described in the Results section and expressed in terms of E, the fraction of excited donors that transfer their energy to the acceptors. The distances were obtained from the energy transfer efficiencies (E) by using Förster's equation

$$R = R_0(E^{-1} - 1)^{1/6} \tag{1}$$

where R_0, the Förster distance, is defined as the distance at which energy transfer is 50% and is determined by the equation

$$R_0 = 0.211\cdot[\kappa^2\cdot Q_D\cdot n^{-4}\cdot J]^{1/6} \text{ (in Å)} \tag{2}$$

where Q_D is the quantum yield of FM when covalently reacted with ghosts (measured relative to a fluorescein standard in 0.1 M NaOH; quantum yield assumed to be 0.92 (*31*)), n is the refractive index (assumed to be 1.34), J is the overlap integral, and κ^2 is the orientation factor assumed to be $^2/_3$ (see Discussion). A value of $R_0 = 58$ Å was obtained.

Time-Correlated Single Photon Counting (TCSPC). The measurement of fluorescence lifetimes was performed by the time-correlated single photon counting (TCSPC) method using facilities at the Center for Photoinduced Charge Transfer (CPCT) in the Department of Chemistry, University of Rochester. The fundamental frequency (1053 nm) of a Coherent Antares A76s Nd:YLF cw-modelocked laser was frequency doubled in a KTP (potassium titanyl phosphate) crystal to give a 527 nm, 76 MHz pulse train, which was then used to synchronously pump a Coherent 7000 series Pyridine-1 dye laser. A Coherent 7220 cavity dumper reduced the repetition rate and decreased the pulse width. The output of the dye laser was added to the 1053 nm fundamental frequency in a BBO (beta barium borate) crystal to produce 420 nm light for the excitation of FM. Fluorescence emission was detected at 522 nm by a Microchannel Plate Photomultiplier (MCP/PMT). FM lifetimes were measured at room-temperature, first with FM-ghosts corresponding to 50−100 nM of hAE1 suspended in the relevant buffer and then after adding diTBA (50 nM diTBA per 20 nM hAE1). The instrument response function was obtained from light scattering signals at the excitation wavelength. Data acquisition, deconvolution and exponential fitting were performed with an FLA9000 software package (Edinburg Analytical Instruments, Livingston, UK).

The deconvoluted fluorescence lifetime decay data were fitted to the following equation

$$I(t) = B + \sum a_i \exp(-t/\tau_i) \tag{3}$$

where I(t) is the fluorescence intensity at time t, B is the background count, and a_i is the preexponential factor for lifetime τ_i. All lifetimes are reported as averages calculated by the following equation

$$\langle\tau\rangle = \sum \frac{a_i\cdot\tau_i^2}{\sum a_i\cdot\tau_i} \tag{4}$$

RESULTS

External Labeling of Red Blood Cells with Fluorescein Maleimide. Labeling of intact red blood cells with FM under the conditions described in Experimental Procedures causes inhibition of anion exchange in RBCs, as measured by ^{36}Cl self-exchange (Figure 2A). The degree of inhibition was ∼35% when FM labeling was performed with 50% hematocrit and ∼50% when performed at 25% hct. This partial inhibition of anion exchange activity could be explained as either a partial inhibition of each hAE1 molecule's anion exchange activity by FM labeling or a fractional labeling of the available hAE1 sites by FM. The stoichiometry of FM labeling per hAE1 monomer, determined by measuring the optical density of FM labeled ghosts solubilized in SDS and taking into account the specificity of FM labeling from fluorescent gels (see below), agrees quite well with the fractional inhibition of anion exchange, providing evidence that the observed partial inhibition of anion exchange reflects the fact that only a fraction (35−50%) of hAE1 monomers are labeled by FM.

Because the majority of hAE1 in the membrane is in the form of dimers, the lack of complete labeling by FM might be explained by an allosteric effect of the FM reaction with one monomer preventing its reaction with the adjacent monomer. However, as shown in Figure 2B, repeated labeling of red blood cells with fresh FM solution leads to a higher inhibition of anion exchange activity (solid squares) than when the cells are exposed to a single FM solution for the same total time (open circles). Moreover, after five consecutive treatments with 2 mM FM, the anion exchange activity is inhibited by about 92% (triangles in Figure 2B), and the data fits well to a single-exponential function (dotted line) with a rate constant of 0.0077 min^{-1} with no uninhibitable component, providing no evidence for negative cooperativity. Spectroscopic data (Figure 3) show that in an aqueous solution, under the conditions used for labeling (open circles), FM tends to hydrolyze rapidly to form a nonreactive product that exhibits higher fluorescence intensity at 522 nm when excited at 492 nm. This behavior resembles that of a FM analogue, eosin-5-maleimide (EM) (*32*). The hydrolysis is slower at lower pH (solid squares), but lowering the pH would also reduce the reactivity of the amino groups

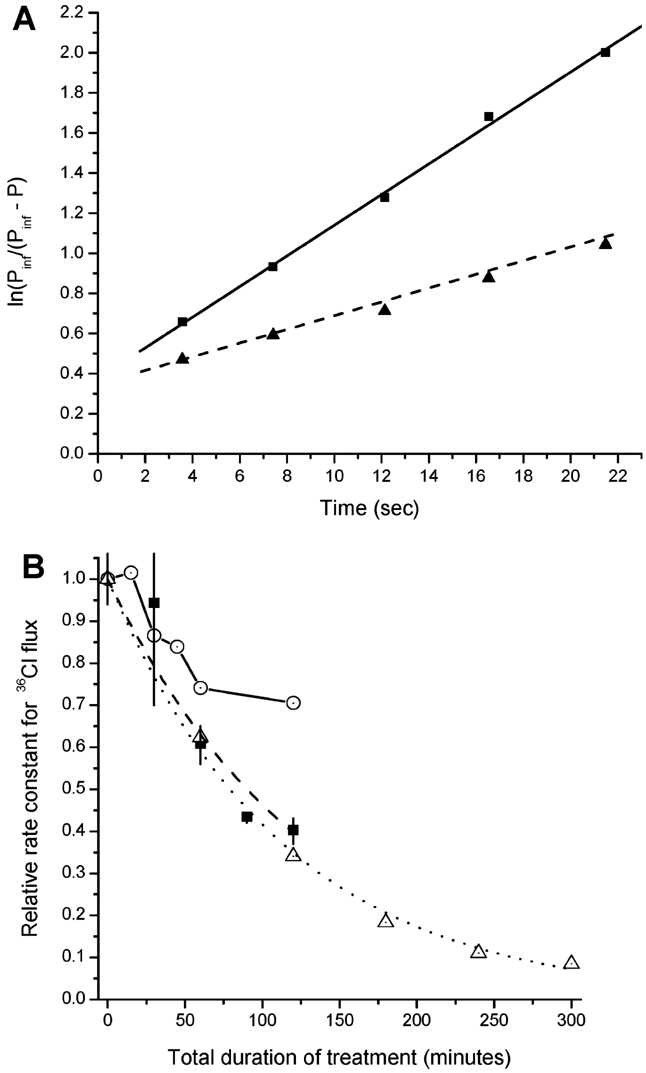

FIGURE 2: Inhibition of ^{36}Cl flux in red blood cells after FM labeling. (A) ^{36}Cl fluxes were measured as described in Experimental Procedures in FM-labeled (▲) or control (■) red blood cells. Solid and dashed lines represent linear fits to the data. The rate constants for Cl^- self-exchange, obtained from the slopes, are 0.074 s^{-1} for the control and 0.032 s^{-1} for the FM-labeled red blood cells. (B) Rate constants in various FM-treated cells normalized relative to the rates in untreated cells for each experiment, showing a single treatment with 1.2 mM FM (○) for the times indicated, multiple treatments (each 30 min) with 1.2 mM FM (■), and multiple 1 h treatments with 2mM FM (△). The latter two data sets fit well to single exponentials, with apparent reaction rate constants of 0.0077 min^{-1} (----) and 0.0088 min^{-1} (....) and with no FM-resistant flux component.

with FM. Thus, the partial labeling resulting from a single FM treatment is probably due to the gradual depletion of the reactive dye by hydrolysis rather than to the negative cooperativity between adjacent monomers. For subsequent steady state FRET studies, ghost membranes prepared from RBCs with approximately 50% inhibition of anion exchange were used.

To determine the location of FM binding to hAE1, the FM-ghosts were subjected to chymotrypsin digestion, followed by trypsin digestion, with subsequent SDS−PAGE separation and detection of FM by fluorescence (Figure 4A). Chymotrypsin cleaves in the third extracellular loop of the hAE1 membrane domain after Tyr-555, whereas trypsin cleaves at Lys-360 to remove the cytoplasmic domain (Figure

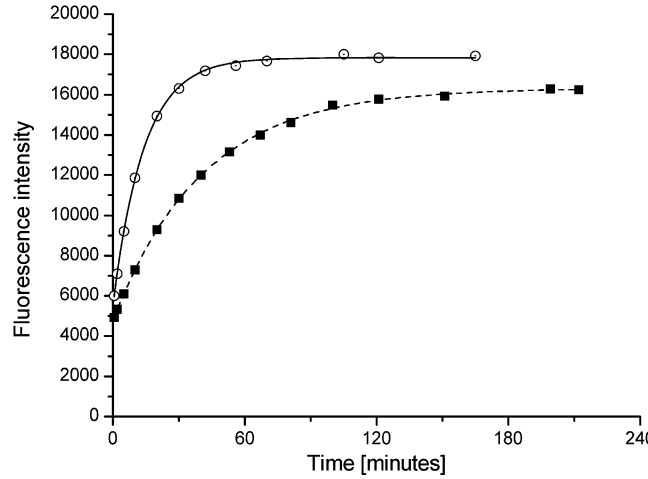

FIGURE 3: Hydrolysis of FM in aqueous buffer. Fluorescence intensity of 100 nM fluorescein maleimide dissolved in 162KH at pH 8.0 (○) or pH 7.4 (■) and incubated at 37 °C was measured as a function of time with excitation at 492 nm and emission summed from 500 to 560 nm. The gradual increase in intensity indicates a hydrolyzed product, which is apparently nonreactive. Exponential fits yield reaction rate constants of 0.071 ± 0.001 min^{-1} at pH 8 (—) and 0.025 ± 0.001 min^{-1} at pH 7.4 (----).

4B). The combination of these treatments produces a 17 kDa *N*-terminal (adjacent to the cytoplasmic domain) and a 38 kDa *C*-terminal segment of the hAE1 membrane domain. Most of the fluorescence is associated with the band near 17 kDa. This is consistent with previous trypsin cleavage results for hAE1 labeled with external FM (*33*) and is the same hAE1 segment labeled by the FM congeners, EM, and iodoacetamido-eosin (*34*, *35*). For these labels, the sequencing of the labeled product reveals that the site of reaction is Lys-430. Although there is a cysteine present in this segment, Cys-479, this cysteine is unreactive with sulfhydryl reagents, including EM, iodoacetamido-eosin, and even *N*-ethyl maleimide (*36*). Although the product of the reaction with FM has not been sequenced, the structural similarity between FM and EM makes it highly likely that the labeling site for FM is also Lys-430. For convenience, we will refer to the external FM labeling site as Lys-430; should this not be the case, the conclusions of this paper are not affected, except insofar that the identity of the benchmark FM site would be different.

Steady-State Fluorescence Energy Transfer from FM to diTBA. The basic principle of the FM−diTBA intermonomer energy transfer measurements is shown as a cartoon in Figure 5. Briefly, in the ghost membranes made from FM-labeled RBCs with 50% inhibition (hereafter referred to as FM-ghosts), assuming random reaction between FM and hAE1 (because there is no evidence for negative cooperativity), a binomial distribution of FM labeling is expected in hAE1 dimers, that is, roughly 25% of the dimers will have FM on both monomers (FF) and another 25% will have no labeling at all (EE). The remaining 50% will have only one monomer labeled with FM (FE), as depicted in the upper panel in Figure 5. The FM serves as an energy transfer donor in these experiments, and diTBA, a fluorescent oxonol that binds noncovalently to hAE1 with very high affinity (K_d ∼12 nM measured by inhibition of chloride fluxes at 0 °C), serves as an acceptor.

Thus, when diTBA is added to the FM-ghosts, it binds to the empty monomer adjacent to the one containing the FM in an FE dimer (Figure 5, middle panel). The excitation of

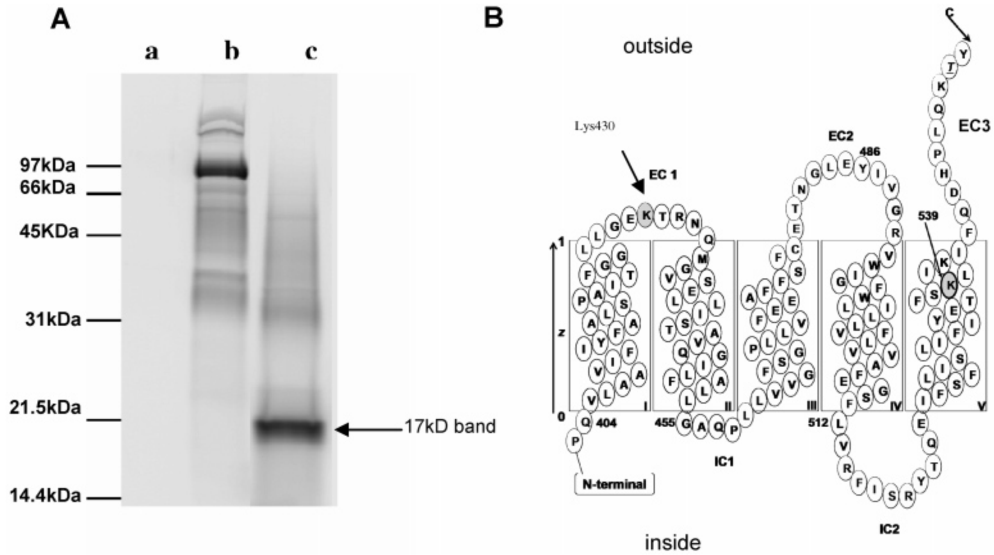

FIGURE 4: Location of the exterior FM binding site. (A) SDS−PAGE gel viewed by fluorescence. Ghost membranes from (a) unlabeled red cells (b) FM-labeled cells, and (c) FM-labeled ghost membranes treated with chymotrypsin (100 μg/mL for 1 h at 20 °C) followed by trypsin (25 μg/mL for 30 min at 0 °C). The 17 kDa band containing the majority of fluorescence is indicated by the arrow. (B) Topology of the first five transmembrane regions (indicated by Roman numerals at the lower right corners of the rectangles) of the membrane domain of AE1. The ICs and ECs refer to intracellular and extracellular loops, respectively. The chymotrypsin cleavage site in EC3 is shown by C and the location of Lys-430 in EC1 is pointed out by an arrow. The location of Lys-539, the site for DIDS reaction, is also shown.

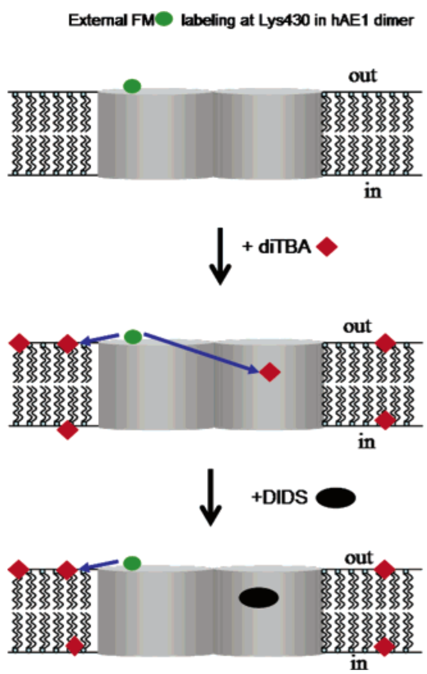

FIGURE 5: Cartoon showing experimental scheme for FM-diTBA intermonomer energy transfer experiment. The top diagram shows a hAE1 dimer in the membrane with one monomer labeled by FM (small oval). When diTBA (diamond) is added, it binds specifically to the adjacent monomer as well as nonspecifically to the membrane. At this time, FM is quenched by energy transfer to both forms of bound diTBA. After the addition of DIDS (large oval), the hAE1-bound diTBA is displaced, and FM is quenched only by the nonspecifically bound diTBA.

FM will cause energy transfer to take place from the FM in one monomer to the diTBA in the adjacent monomer. This energy transfer is referred to as specific energy transfer (SET). As indicated in Figure 5, diTBA also tends to bind nonspecifically to the lipid bilayer, which is expected because oxonols are used as probes for sensing membrane potentials (*37*). Hence, there is some energy transfer from FM on both FE and FF dimers to the non-hAE1-bound diTBA. This is referred to as nonspecific energy transfer (NSET). To distinguish between SET and NSET, a disulfonic stilbene inhibitor of hAE1, DIDS, is subsequently added (Figure 5, bottom panel). DIDS covalently binds to hAE1 and displaces the hAE1-bound diTBA molecules (*38*), leaving only the NSET components. Deconvolution of the SET and NSET components from the observed fluorescence intensities is described below.

The situation is simplified by evidence that binding of diTBA and FM to the same hAE1 monomer is mutually exclusive as shown in Figure 6. Figure 6A shows data for the binding of diTBA to ghosts from control cells or cells that have been reacted with 1.2 mM FM for 1 h as shown in Figure 2B and described in Methods. The binding of diTBA to hAE1 causes an increase in the quantum yield, as reflected by an exponential increase in fluorescence as binding approaches equilibrium. The addition of DIDS, which competes with diTBA, causes the release of the diTBA from its hAE1 binding sites and a corresponding decrease in fluorescence. The reaction with FM reduces the fluorescence increase, consistent with the hypothesis that diTBA cannot bind to the hAE1 monomer that has reacted with FM. This is shown more clearly in Figure 6B, where the fluorescence due to hAE1-bound diTBA is shown, determined by subtracting the fluorescence after DIDS treatment (due to nonspecifically bound diTBA and diTBA in solution) from the total fluorescence.

Further evidence that FM binding to a hAE1 monomer prevents diTBA binding to that monomer comes from an analysis of the fluorescence after DIDS addition. Stilbene disulfonates such as DIDS are mutually exclusive with EM or FM (*35*); therefore, hAE1 monomers that have reacted with FM cannot bind DIDS. Thus, if diTBA were bound to an FM-reacted hAE1 monomer, it could not be displaced by DIDS, and therefore, the residual fluorescence after DIDS addition would be higher for the FM-reacted cells. Figure

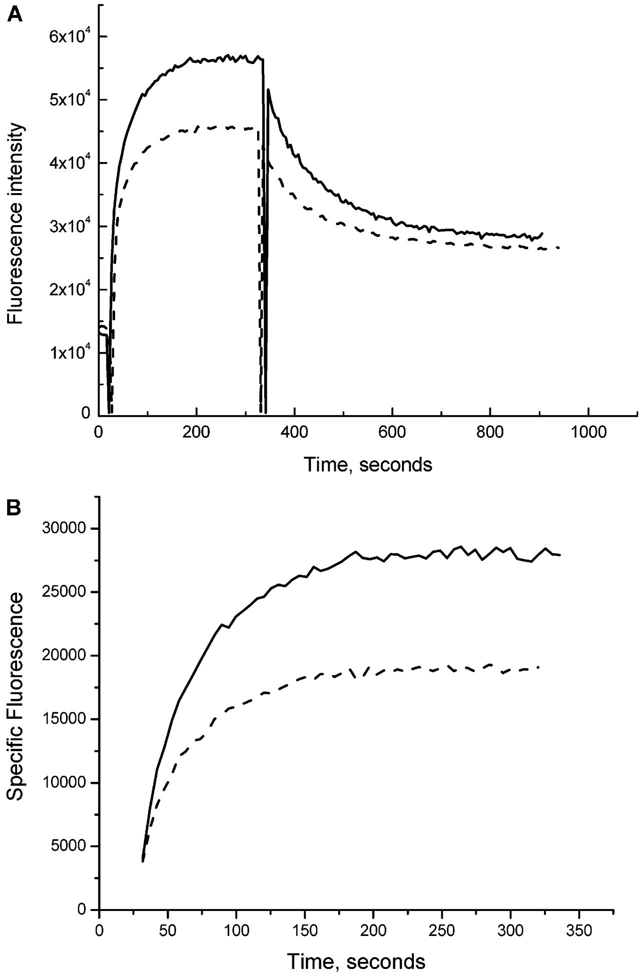

FIGURE 6: (A) Effects of external FM labeling on diTBA binding. Ghosts from RBCs that underwent a single 1 h treatment with 1.2 mM FM (----) (Experimental Procedures) or no treatment at all (control cells) (—) containing 4 nM hAE1 were added to 50 nM diTBA in a 150KH medium (0 °C), and the binding was later reversed by adding 1 μM DIDS. Samples were excited at 535 nm, and emission was monitored at 560 nm to observe diTBA emission. Upon the addition of ghosts, the emission intensity of diTBA goes up because of binding to hAE1. FM labeling of ghosts reduces this increase, indicating that diTBA and FM binding are mutually exclusive. After the addition of DIDS, the diTBA fluorescence goes down and reaches a plateau. The plateau represents diTBA fluorescence from nonspecifically bound diTBA and diTBA in solution. (B) This plateau is subtracted from the fluorescence emission at 560 nm prior to the addition of DIDS to show the specific diTBA binding. Control cells (—); FM treated cells (----).

6A shows that this is not the case, providing evidence that the labeling with FM and the binding of diTBA are mutually exclusive.

Figure 7 shows evidence for the energy transfer described above measured by steady state fluorescence emission. The solid line represents the steady state fluorescence emission spectrum of a suspension of FM-ghosts (final hAE1 concentration = 20 nM) in a 150 mM chloride buffer with excitation at 435 nm. This excitation wavelength was chosen rather than the absorption maximum of FM (488 nm) to minimize the direct excitation of the acceptor, diTBA, (dash−dot line) while maintaining an appreciable emission of FM at 522 nm. After the addition of 50 nM diTBA, there is a decrease in FM fluorescence at 522 nm (dotted line) and a concomitant increase in emission at 550−560 nm,

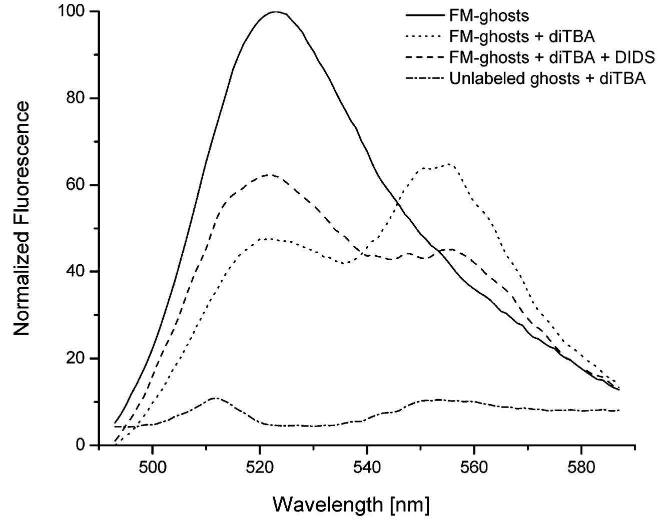

FIGURE 7: Steady state spectra showing FM−diTBA energy transfer experiments. The excitation wavelength was 435 nm. FM-ghosts containing 20 nM hAE1 (~50% labeled) were added to a buffer containing 150 mM sodium chloride and 24 mM HEPES at pH 8.0, and the emission spectra were obtained before (—) and after (....) the addition of 50 nM diTBA and then after the addition of 20 μM DIDS (----). A spectrum was taken after the addition of 50 nM diTBA to unlabeled ghost membranes, showing very little direct excitation of diTBA (•-•-•).

indicating energy transfer from FM to diTBA. As explained above, these changes include effects of FRET from FM to diTBA molecules located at places other than hAE1. To determine how much nonspecific energy transfer is occurring, the covalent disulfonic stilbene inhibitor of hAE1, DIDS, is added, which reacts specifically with hAE1 and displaces the diTBA that is bound to hAE1. Upon the addition of excess DIDS (20 μM) (dashed line), FM emission intensity (at 522 nm) increases, although it is still less than that of the FM-ghosts without diTBA (solid line). There is also a reduction in fluorescence intensity at the diTBA emission wavelength (550−560 nm). This fits with the model in which the quenching of FM fluorescence is due to energy transfer from the hAE1-bound FM both to diTBA bound specifically to hAE1 (SET, DIDS sensitive) and to other diTBA molecules bound to different parts of the ghost membrane, such as to the lipid bilayer or possibly to other proteins (NSET, DIDS insensitive). Experiments performed in bicarbonate or citrate buffers revealed similar trends, although the magnitudes of the observed changes were different, as explained below.

Further evidence that a major component of the quenching of FM fluorescence results from diTBA specifically bound to hAE1 comes from the time course of the fluorescence changes (Figure 8). Figure 8A shows data for FM-ghosts in a 150 mM bicarbonate medium, with excitation at 435 nm and emission measured at either 522 nm (fluorescein, solid line) or 560 nm (diTBA, dashed line). Before the addition of diTBA (0−200 s) some emission is seen at 560 nm because of emission by FM at this wavelength (Figure 7, solid line). Upon the addition of diTBA, the FM fluorescence decreases in parallel with the increase in diTBA fluorescence. In this case, almost all of the diTBA fluorescence is the result of the excitation of diTBA by energy transfer from fluorescein; ghosts from control cells exhibit very little 560 nm fluorescence when excited at 435 nm (Figure 7, dash-dot

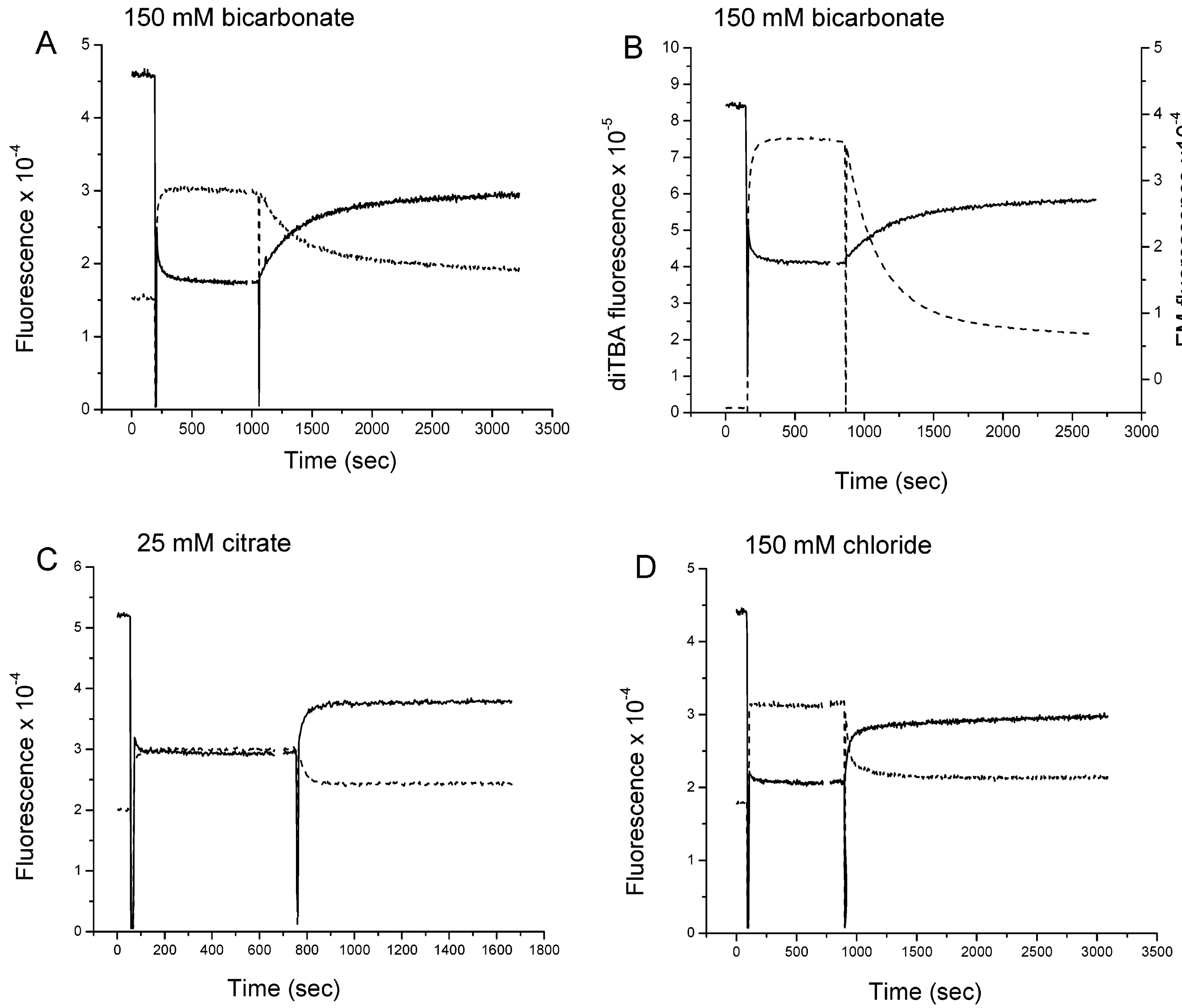

FIGURE 8: Time series showing the FM−diTBA energy transfer in various media by dual channel detection. FM-ghosts containing 20 nM hAE1 were added to 150 mM HCO_3^- (A and B), 25 mM citrate (C), or 150 mM Cl^- (D) buffers (Experimental Procedures) followed by 50 nM diTBA and then 20 μM DIDS. In panels A, C, and D, the samples were excited at 435 nm, and fluorescence was simultaneously monitored at 522 nm (—) for FM donor emission and at 560 nm (----) for stimulated diTBA acceptor emission (emission due to energy transfer). In panel B, the samples were alternately excited at 435 nm with observation at 522 nm (—) for FM emission and at 530 nm with observation at 560 nm (----) for diTBA emission. Note that the diTBA emission in panel B is due to the direct excitation of the acceptor as opposed to the stimulated emission through energy transfer observed in the other panels.

line). The addition of 20 μM DIDS, which reacts with free hAE1 and prevents it from binding diTBA, causes the reversal of the hAE1-specific binding of diTBA, as indicated by the decrease in diTBA fluorescence at 560 nm. This is paralleled by an increase in FM fluorescence at 522 nm, reflecting decreased FM quenching because the energy transfer to hAE1-bound diTBA (SET) decreases as diTBA debinds from hAE1.

Figure 8B shows more clearly that the FM emission changes approximately mirror the changes in diTBA fluorescence due to hAE1 binding and debinding. Here, the dashed line represents directly excited diTBA fluorescence with excitation at 530 nm and emission at 560 nm. Note that in this case the 560 nm fluorescence is very low before the addition of diTBA because FM is not excited by illumination at 530 nm. The fluorescence at 560 nm increases upon diTBA addition (as diTBA binds to hAE1, its intensity increases) in parallel with the quenching of the FM signal (solid line). The addition of DIDS causes a slow decrease in diTBA fluorescence, as diTBA is released from the hAE1 binding site into the medium, where it is less fluorescent. This decrease is accompanied by a parallel increase in FM fluorescence because the removal of diTBA from hAE1 reduces the SET from FM to diTBA and, thus, increases the FM fluorescence.

Figures 8C and D show similar experiments in media with the same ionic strength but with different anions present. The excitation is at 435 nm as in Figure 8A, and the emission is measured at either 522 nm (solid line) or 560 nm (dashed line). In the citrate medium, Figure 8C, hAE1 should be primarily in the form without the substrates bound because hAE1 has a very low affinity for citrate when it is primarily in the trivalent form (at pH 8) (*39*, *40*). In this case, the increase in 560 nm fluorescence after the addition of diTBA and the decrease in 522 nm fluorescence are both smaller than those in bicarbonate media (Figure 8A), and the specific

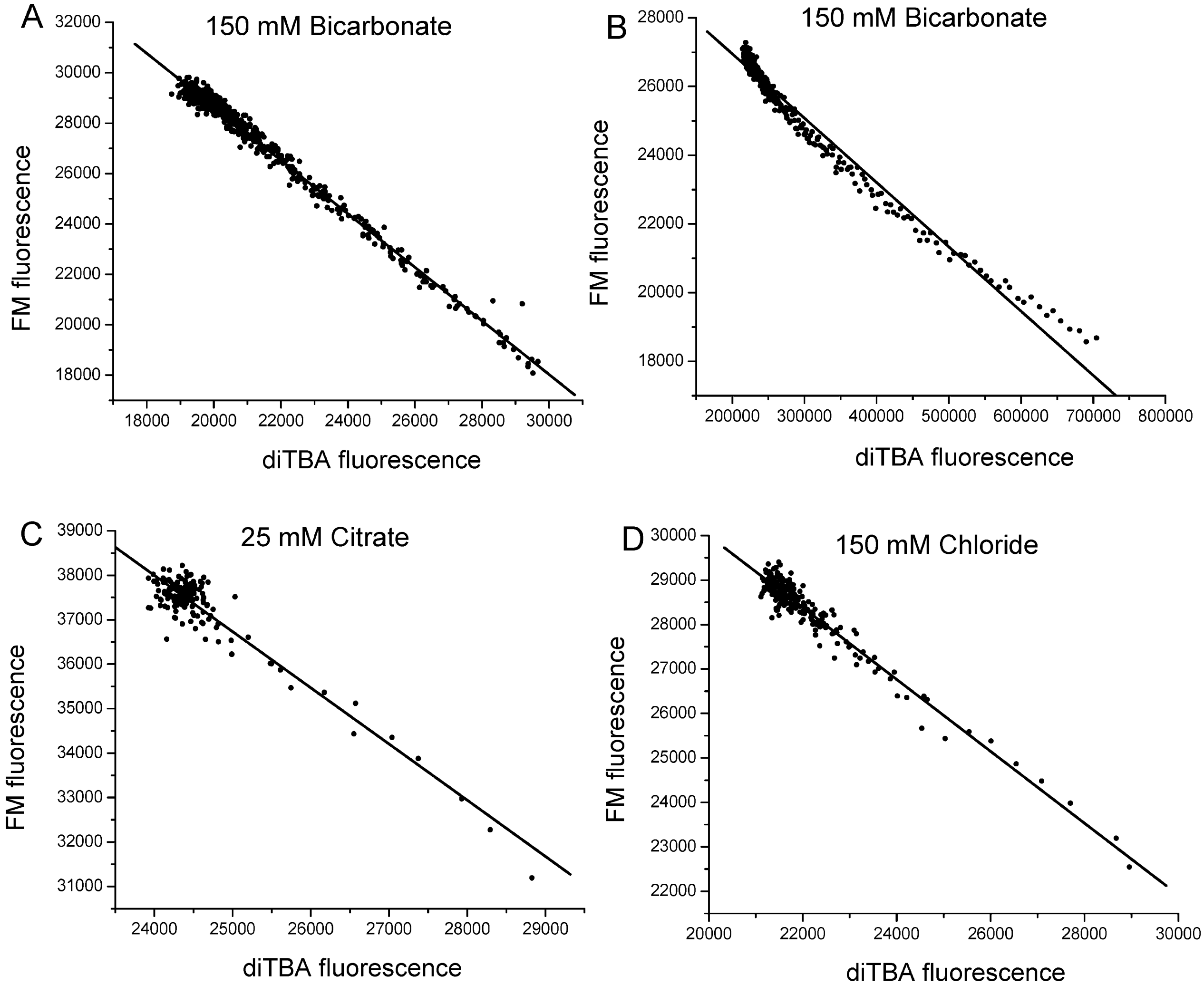

FIGURE 9: Correlation plots of fluorescence at 522 nm (FM, *y*-axis) versus fluorescence at 560 nm (diTBA, *x*-axis) after DIDS binding. Excitation was at 435 nm for both FM and diTBA fluorescence in (A), (C), and (D), and at 435 nm for FM fluorescence and 530 nM for diTBA fluorescence in (B).

energy transfer revealed by reversing hAE1-specific diTBA binding with DIDS is also smaller. The same is true for the 150 mM chloride medium (Figure 8D). Note that in both citrate and chloride the debinding of diTBA after DIDS addition is much faster than in bicarbonate, but the changes in FM and diTBA fluorescence are still completely parallel, providing evidence that the changes in FM fluorescence are due to hAE1-bound diTBA that can be released by DIDS treatment.

Figure 9 shows similar data for FM and diTBA fluorescence after the addition of DIDS but with the FM fluorescence plotted against the diTBA fluorescence for each time point. In Figure 9A, C, and D, where excitation is at 435 nm, the changes in FM and diTBA fluorescence are highly correlated despite their different time courses in the different media. The more rapid fluorescence changes in citrate or Cl^- media are reflected by the less dense distribution of points because each point represents a fixed time interval of fluorescence measurement. As shown in Appendix 1, this behavior is expected either for a homogeneous population of diTBA binding sites or for a mixed population, as long as all of the diTBA molecules have the same quantum yield.

The curvature seen in Figure 9B, where the *x*-axis represents directly excited diTBA fluorescence (excitation 530 nm and emission 560 nm), rather than fluorescence excited by energy transfer from FM, indicates that there is some heterogeneity in the population of diTBA acceptors (Appendix 1). One possible interpretation of the data is that the energy transfer to the diTBA population that debinds more slowly (which will be the dominant population at later times after DIDS addition, corresponding to the part of the plot with high FM fluorescence and low diTBA fluorescence in Figure 9B) is greater than the energy transfer to the more rapidly debinding population. This in turn would indicate that the more rapidly debinding diTBA is bound to conformations of hAE1 in which the diTBA binding site is farther from the FM binding site on the adjacent monomer. Because of such possible heterogeneity, all of the energy transfer efficiencies and corresponding distances should be regarded as effective parameters, which may actually reflect a mixture of the properties of the different conformations of hAE1 that are present under a given set of conditions.

Determination of Fractional Occupancy of diTBA. Because diTBA is a reversible inhibitor of hAE1, not all of the possible diTBA sites (in the FE hAE1 species) are occupied under the conditions of this experiment. Also, the slower rate of diTBA debinding from hAE1 observed in Figure 8A and B in bicarbonate versus chloride or citrate buffers (Figure

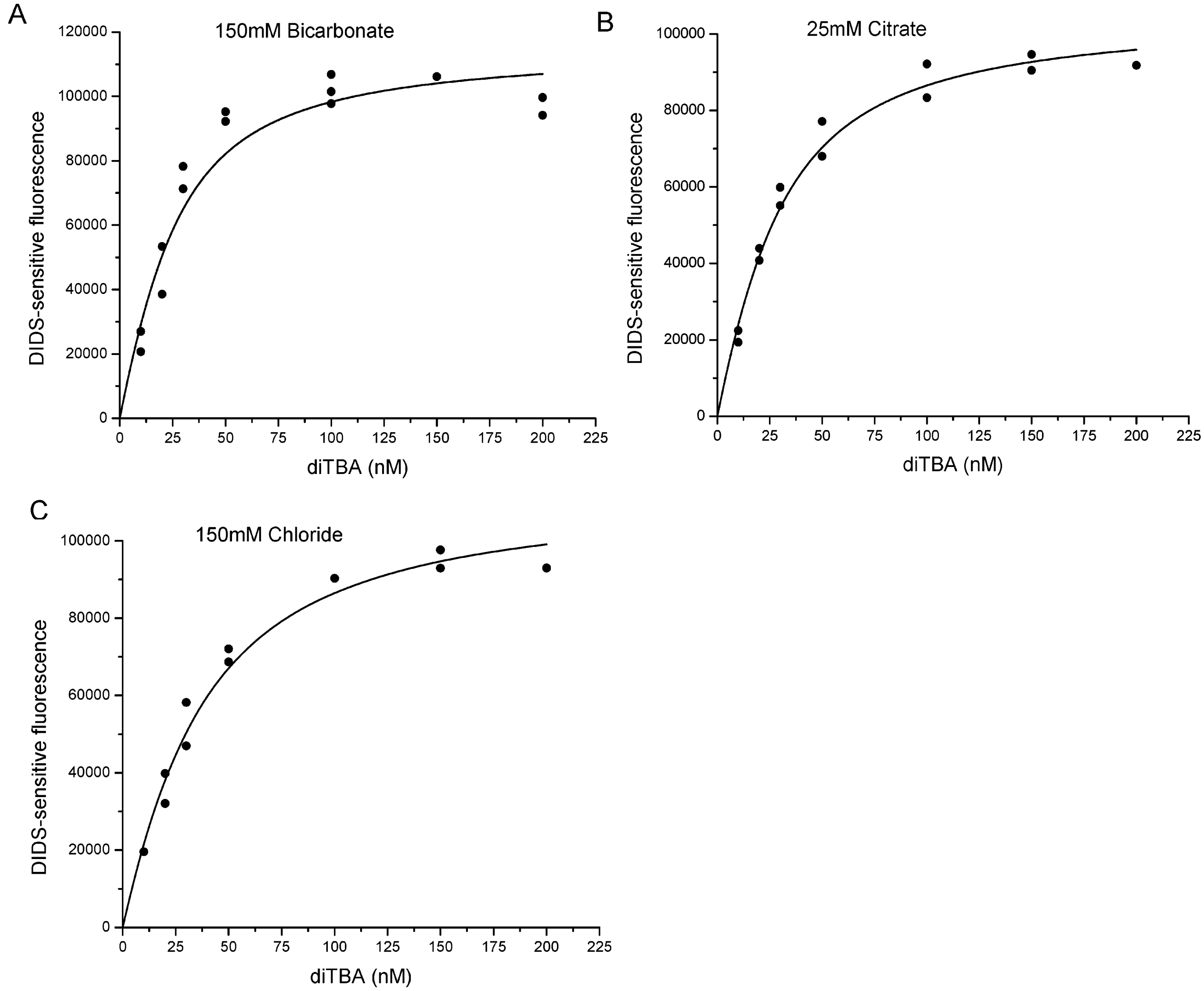

FIGURE 10: Determination of apparent diTBA binding affinity in different buffers. Ghosts containing 20 nM hAE1 were added to different amounts of diTBA in (A) bicarbonate, (B) citrate, or (C) chloride buffers. The total fluorescence enhancement due to both specific and nonspecific binding was measured. The specific component was then removed by the addition of 20 μM DIDS. The difference in fluorescence before and after DIDS addition was plotted as DIDS-sensitive fluorescence against diTBA concentration. Data were fitted by a modified Michaelis−Menten equation that considers the depletion of diTBA (Appendix 2). Fitted apparent K_d values (K_d') are 16.7 ± 0.2 nM for citrate, 27.9 ± 4.4 nM for chloride, and 14.5 ± 0.1 nM for bicarbonate (values are mean ± SEM).

8C and D) suggests that the affinity of diTBA for hAE1 sites might be different in various buffers. This would result in different fractional occupancies (*f*) of the hAE1 sites in different buffers for the same amount of diTBA added. Because such a fractional occupancy would affect the FRET measurements, the apparent dissociation constants of the hAE1-specific diTBA binding were determined under the experimental conditions used for FRET.

To do this, steady state fluorescence intensity was measured over time with excitation at 530 nm and emission at 560 nm. The desired amount of diTBA was first added to the cuvette, followed by the addition of unlabeled ghosts containing 20 nM hAE1, which causes an enhancement of the diTBA fluorescence due to both specific and nonspecific binding. To determine the specific (DIDS-sensitive) binding, 20 μM DIDS was added. The DIDS-sensitive fluorescence was plotted as a function of diTBA concentration (Figure 10) and the apparent dissociation constant determined by using a Michaelis−Menten type equation that takes into account the depletion of free diTBA due to specific and nonspecific binding (Appendix 2). The measured apparent dissociation constants were 16.7 ± 0.2 nM for citrate, 27.9 ± 4.4 nM for chloride, and 14.5 ± 0.1 nM for bicarbonate. These correspond to fractional occupation values with 50 nM diTBA of 0.72, 0.61, and 0.75 for citrate, chloride, and bicarbonate, respectively.

Quantification of the Specific Energy Transfer Component. As mentioned above, because there was no evidence for any cooperative effects of FM labeling, there should be a binomial distribution of the hAE1 dimers labeled with two FM (FF), one FM (FE), or with no FM at all (EE). The quenching of FM in the FF species will be due to NSET only, although both SET and NSET mechanisms will cause quenching in the FE dimers. By using the fractional inhibition of the anion exchanger as a measure of the hAE1-specific FM binding, the distribution of these species and, therefore, their contribution to the FM fluorescence intensity can be calculated.

If the fluorescence intensity of FM, measured at 522 nm in FM-labeled ghosts before the addition of diTBA, is defined as F_A, after the addition of diTBA as F_B, and after the addition of DIDS as F_C, and the fractions of hAE1 dimers that are labeled by two FMs or one FM are defined as P_{FF} and P_{FE}, respectively, then

$$F_A = Q_D(2P_{FF} + P_{FE})[b3D] \quad (5a)$$

$$F_B = (2Q_{DN}\cdot P_{FF} + (1 - f)Q_{DN}\cdot P_{FE} + f\cdot Q_{DS}\cdot P_{FE})[b3D] \quad (5b)$$

$$F_C = Q_{DN}(2P_{FF} + P_{FE})[b3D] \quad (5c)$$

where $[b3D]$ is the concentration of the hAE1 dimers, and f is the fractional occupation of hAE1 sites by diTBA. Q_D, Q_{DN}, and Q_{DS}, the quantum yields of donors in the absence of FRET, with FRET to nonspecifically bound diTBA, or with FRET to both nonspecific and hAE1-bound diTBA, respectively, are defined as

$$Q_D = \frac{k_f}{k_f + k_{nr}} \quad (6a)$$

$$Q_{DN} = \frac{k_f}{k_f + k_{nr} + k_{TN}} \quad (6b)$$

$$Q_{DS} = \frac{k_f}{k_f + k_{nr} + k_{TN} + k_{TS}} \quad (6c)$$

where k_f is the rate of fluorescence emission, k_{nr} is the rate of excited-state decay by nonradiative processes, k_{TN} is the rate of energy transfer to nonspecific (non-hAE1-bound) acceptors, and k_{TS} is the rate of energy transfer to the specific (hAE1-bound) acceptors. Rearranging equations (5a−c), we obtain

$$\frac{Q_D}{Q_{DN}} = \frac{F_A}{F_C} \quad (7a)$$

$$\frac{Q_D}{Q_{DS}} = \frac{F_A\cdot P_{FE}\cdot f}{2P_{FF}(F_B - F_C) + F_B\cdot P_{FE} - (1 - f)F_C\cdot P_{FE}} \quad (7b)$$

E_S and E_{NS}, the efficiencies of specific and nonspecific energy transfers, respectively, are defined as

$$E_S = \frac{k_{TS}}{k_f + k_{nr} + k_{TS}} \quad (8a)$$

$$E_{NS} = \frac{k_{TN}}{k_f + k_{nr} + k_{TN}} \quad (8b)$$

From eqs 6 and 8, we obtain

$$E_S = \frac{\dfrac{Q_D}{Q_{DS}} - \dfrac{Q_D}{Q_{DN}}}{1 + \dfrac{Q_D}{Q_{DS}} - \dfrac{Q_D}{Q_{DN}}} \quad (9a)$$

$$E_{NS} = 1 - \frac{Q_{DN}}{Q_D} \quad (9b)$$

Both E_S and E_{NS} can be calculated from eqs 9a and b by substituting the values for Q_D/Q_{DS} and Q_D/Q_{DN} from eqs 7a and b, which are expressed in terms of the observable F_A, F_B, and F_C and the measurable factor f. To obtain these values, the effects of the sequential addition of diTBA and DIDS on FM fluorescence intensity at 522 nm were measured (as in Figures 7 and 8). The decrease in FM fluorescence after the addition of diTBA and the subsequent increase after the addition of DIDS both follow an exponential time course. Once the fluorescence reached an apparent plateau after each addition, the intensity was averaged over a time interval of 100 or 200 s.

Table 1: Specific and Nonspecific Energy Transfer Values and Intermonomer FM−diTBA Distances[a]

	specific		nonspecific
	energy transfer (%)	distance (Å)	energy transfer (%)
citrate ($n = 3$)	53.1 ± 0.6	56.8 ± 0.3	7.5 ± 1.1
chloride ($n = 6$)	71.4 ± 2.1	49.8 ± 0.9	16.8 ± 2.0
bicarbonate ($n = 4$)	79.7 ± 0.6	46.2 ± 0.3	13.5 ± 4.3

[a] Specific energy transfer distance refers to the intermonomer distance between FM on one monomer and diTBA on the adjacent monomer of a hAE1 dimer. The distances are calculated using eq 1 and the calculated $R_0 = 58$ Å. Because of the multiplicity of acceptors, the distances for nonspecific energy transfer (NSET) cannot be calculated. All values are reported as mean ± standard error of mean of values obtained from n separate experiments. All distance and energy transfer values are significantly different ($p < 0.05$) from each other except for the nonspecific energy transfer values in chloride and bicarbonate.

As reported in Table 1, the specific energy transfer efficiency values determined in this manner in a citrate buffer give an average SET of 53.1%. The nonspecific energy transfer as calculated by this method was 7.5, 16.8, and 13.5% in citrate, chloride, or bicarbonate, respectively. Hence, there is a small increase in the NSET in chloride or bicarbonate as compared to that in citrate. The SET, however, increased substantially to 71.4% in the chloride buffer, and there was a further statistically significant increase in SET to 79.7% in the bicarbonate buffer. The SET efficiencies in chloride or bicarbonate determined with 50 nM diTBA agree with the SET values obtained with 100 nM diTBA, indicating that the effect of the fractional occupation of diTBA sites was properly taken into account in the calculations.

If κ^2 is assumed to be $^2/_3$, then these observations indicate that the FM−diTBA intermonomer distance is the shortest in bicarbonate buffers (46.2 Å), increases slightly in chloride (49.8 Å), and is the maximum in citrate (56.8 Å). It is also possible that there is a reorientation of the fluorescent probes, which changes κ^2 and, thus, gives rise to the stronger energy transfer in bicarbonate and chloride versus citrate. In either case, the data demonstrates that some conformational rearrangement has occurred because of the presence of transportable anions in the buffer.

Fluorescence Lifetime Measurements. To confirm the findings from steady state measurements as well as to determine if there are any direct effects of the different anions on the properties of the fluorescein donor, TCSPC measurements (Experimental Procedures) of FM lifetime were performed. The emission lifetime data for FM-ghosts in different buffers could be fitted to either a monoexponential or a biexponential decay, with slightly better reduced χ^2 values for the biexponential fit (for example, 1.14 versus 1.20 for an experiment in the citrate buffer). The longer lifetime component, 4.15 ns in citrate, was relatively constant, whereas the lifetimes of the shorter component varied from 0.6 to 1.7 ns. In terms of amplitude, the latter component

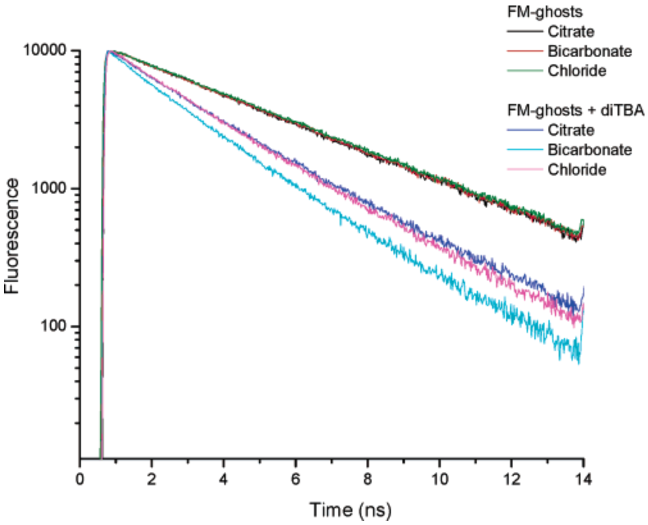

FIGURE 11: Plots of FM fluorescence lifetime. The lifetime of FM measured in FM-ghosts is similar in all of the buffers before the addition of diTBA (upper lines). After diTBA addition, the maximum quenching (decrease of lifetime) was observed in HCO_3^- and the least quenching in citrate.

was very small, contributing only to 2−5% of the total population. This short lifetime could be caused by the presence of some nonspecific (non-hAE1-bound) FM or could even be due to a minor artifact[2] in the SPC instrument. To avoid bias, average lifetimes calculated as described in the Experimental Procedures section were used. As shown in Figure 11, there is no significant ($p < 0.05$) difference in the average lifetimes of the FM-ghosts in citrate (4.15 ± 0.03 ns), bicarbonate (4.16 ± 0.03 ns), or chloride (4.18 ± 0.01 ns) buffers ($n = 3$ in all cases). This indicates that there is no effect on the environment of the FM attached to hAE1 when different anions are present. The FM lifetime values agree with data reported elsewhere (*29*, *33*).

As expected, after the addition of diTBA, the lifetime of FM is reduced (Figure 11) because of energy transfer. The best fit, in this case, was obtained with a three-exponential fit that included one very small component (lifetime <0.6 ns and amplitude 1−7%). The quenched lifetime of FM in the presence of diTBA should ideally have two components: the NSET-only quenched FM ($\tau = 3.5$−3.8 ns based on 7−16% NSET values observed from the steady state experiments above) due to the FF dimers and the SET (and NSET)-quenched FM ($\tau = 2.15$ ns, based on ∼50% energy transfer for citrate, shorter in other buffers) arising from the FE dimers. Such closely spaced lifetime values cannot be resolved accurately by exponential fitting methods. Therefore, we are limited to calculating the average lifetime, which includes both components.

The fractional occupancy of diTBA is similar in citrate and bicarbonate (0.72 and 0.75); therefore, the average quenched lifetime of FM in these two buffers should primarily reflect the difference in the FM−diTBA distances and not the fractional occupancy. As shown in Figure 11, there is a stronger quenching (shorter lifetime) in the bicarbonate buffer ($\langle\tau_{DA}\rangle = 2.47 \pm 0.05$ ns) as compared to that in the citrate buffer ($\langle\tau_{DA}\rangle = 2.92 \pm 0.01$ ns). In chloride, the lifetime is reduced to a smaller extent ($\langle\tau_{DA}\rangle = 2.76 \pm$ 0.01ns) compared to that in citrate, but the difference is statistically significant at $p < 0.05$. In chloride, however, the fractional occupation of diTBA is much lower (0.61) than that in citrate, which means that a greater number of the FM fluorophores have no diTBA in the adjacent monomer to which they can transfer energy, leading to a higher average lifetime.

When the fractional occupancy of diTBA is taken into account, the time-resolved measurements qualitatively agree with the steady state measurements, indicating that there is greater quenching of FM fluorescence by diTBA in bicarbonate and chloride as compared to that in the citrate buffer. The measurements also confirm that there is no significant change in the quantum yield of fluorescein in the different buffers in the absence of diTBA.

DISCUSSION

Effects of Fluorophore Orientation on Distance Measurements. The relative orientation of the fluorophores could affect the absolute distance measurements due to uncertainty in the value of κ^2. It is known that FM bound at Lys-430 has a residual anisotropy of 0.24 in 150 mM chloride (*33*), which corresponds to the fluorophore rotation in a cone with an effective semiangle of 38°, thereby excluding the absolute worst case scenario when $\kappa^2 = 0$. However, because of the high binding affinity and the evidence that a protein conformational change locks diTBA into its binding site, it is likely that diTBA has little or no freedom of motion. On the basis of the methods described by Dale et. al. (*34*), the extreme limits of the distance measured in the Cl^- medium (49.8 ± 0.9 Å) would be 37−65 Å, assuming that diTBA is rigid. Any segmental motion of the protein at the diTBA binding site will reduce the diTBA anisotropy and, hence, the possible range of the absolute FM−diTBA distance.

Nature of Conformational Change. This large uncertainty in the absolute distance between the FM labeling site and the diTBA binding site in the adjacent monomer does not, however, affect the evidence for a substrate-induced change in hAE1 conformation. Table 1 shows that there are significant changes in specific energy transfer when the citrate medium is replaced by either chloride or bicarbonate media. If R_0 is assumed to be constant and to have the value expected for random orientation of the donor and acceptor transition dipoles with $\kappa^2 = {}^2/_3$, then the changes in energy transfer would correspond to the distance changes shown in Table 1. Thus, the FM−diTBA intermonomeric distance would decrease by ∼ 7 Å when Cl^- replaces citrate and ∼10.6 Å when bicarbonate replaces citrate.

Although the other factors that affect R_0 are expected to remain constant in the various anionic media and FM anisotropy is unaffected by anion substitution at constant ionic strength (*33*), changes in the orientation of diTBA could alter κ^2 in such a way as to explain the observed changes in energy transfer. In this case, the substrate-induced conformational change would involve a change in diTBA orientation, rather than a change in the FM−diTBA distance, but there would still be direct evidence for an effect of substrates on hAE1 conformation. For convenience, we will discuss the conformational changes in terms of distance changes at

[2] We have observed a small second excitation laser pulse in some of our measurements after the first excitation pulse. The second lifetime in our analysis could be because of errors caused by the improper deconvolution of the decay data due to this second pulse.

Table 2: Distribution of HAE1 Conformations[a]

		E_o	EX_o	E_i	EX_i	$EX_i + EX_o$	$E_o + EX_o$
$-$I[b]	citrate	5.5	0.3	**94.2**	<0.1	0.3	5.8
	Cl^-	1.3	9.5	21.4	**67.8**	77.3	10.8
	HCO_3^-	1.0	**74.5**	17.0	7.5	82.0	75.5
$+I_{oo}$[c]	citrate	**70.3**	3.5	26.2	<0.1	3.5	73.8
	Cl^-	7.6	**57.5**	8.4	26.5	84.0	65.2
	HCO_3^-	1.2	**92.6**	4.3	1.9	94.5	93.9
+I[d]	citrate	31.0	0.3	**68.7**	<0.1	0.3	31.3
	Cl^-	14.7	19.5	28.8	**37.1**	56.5	34.2
	HCO_3^-	5.8	**79.5**	12.2	2.4	82.0	85.3

[a] X represents either substrate anion, Cl^- or HCO_3^-; all values indicate the percentage of total hAE1 in the indicated forms with 50 nM diTBA and 20 nM hAE1. The most prevalent form is shown in bold. In the case of citrate, we assume that some bicarbonate (0.1 mM) is present (hence, in this case, X = HCO^-_3). Calculations are based on the following parameter values: $A = E_o/E_i = 0.58892$, $A_{Cl} = 0.14$, $A_B = 10$; dissociation constants for Cl^- and HCO_3^- (with Xi = Xo) are 44 mM and 33 mM, respectively. These parameters come from the self-consistent model for Cl/B exchange based on data at 0 °C (*22*). Limited data at 38 °C indicate similar model parameters (*23*). For each case (see below), we used an iterative method to determine the value of the dissociation constant for diTBA binding to the E_o form that was consistent with the fractional occupancies for this experimental condition determined in Figure 10. [b] The $-$I condition represents the case where the binding of diTBA has no effect on the distribution of hAE1 among its various conformations, that is, the binding affinity is the same for each conformation. In this case, the distribution of conformations is exactly the same as what it would be without an inhibitor present and, hence, the $-$I designation. [c] For the $+I_{oo}$ condition, diTBA is assumed to bind only to the outward-facing forms, E_o and ECl_o, and to have the same affinity for both of these forms. [d] For the +I condition, the dissociation constants for diTBA binding to the various hAE1 conformations were assumed to be proportional to those observed for the analogous oxonol, WW781 (*21*). The K_d values for WW781 were taken to be 3.9 nM for E_o, 46 nM (the minimal value observed) for E_i, and 26 nM and 280 nM for EX_o and EX_i, respectively, on the basis of the values observed for iodide-loaded E_o and E_i.

constant R_0, but it should be borne in mind that the data could just as easily be interpreted in terms of changes in diTBA orientation.

To interpret the differences in terms of structural changes occurring during the anion exchange cycle, it is necessary to consider the conformational distribution of hAE1 in the various buffers. Because the energy transfer is measured after the diTBA binding to hAE1 has reached equilibrium, the distribution of hAE1 conformations may be affected by diTBA. It is known that the binding affinities of an oxonol analogous to diTBA, [3-methyl-1-*p*-sulfophenyl-5-pyrazolone-(4)]-[1,3-dibutylbarbituric acid]-pentamethine oxonol (WW781), depend on whether the anion transport site is in the inward (E_i) or outward (E_o) facing form (Figure 1), with a higher affinity observed for the E_o forms (*21*). Because these binding constants are not known for diTBA, three possible effects of diTBA on hAE1 conformational distribution were considered, as enumerated in Table 2. If diTBA has no effect, that is, if the binding affinities of all forms of hAE1 for diTBA are the same, then the conformational distribution would be as shown in Table 2 for the $-$I rows. Because WW781 exhibits a preference for the E_o forms, it is probable that diTBA will also tend to recruit hAE1 toward the outward-facing forms. In the extreme case where diTBA is assumed to bind only to outward-facing forms of hAE1 (loaded or unloaded) but has no affinity for the inward-facing forms, the distribution of conformations will be as in the rows +I only out ($+I_{oo}$). Perhaps the most likely situation is shown in the rows marked +I, where it is assumed that the diTBA binding constants for the different hAE1 conformations have the same relative values as those estimated for WW781.

In addition to the percentage of hAE1 in each form, Table 2 also shows the percentage of sites in the substrate-loaded (inward- or outward-facing) forms and the percentage of sites in the outward-facing (loaded or unloaded) forms. As expected, the percentage of substrate-loaded sites is low when the nontransportable anion citrate is present (in fact, the reason that there are any loaded forms at all in citrate is because we assumed that there is a small amount of bicarbonate (0.1 mM) present in the buffer because of atmospheric CO_2). When Cl^- replaces citrate, a large increase in the Cl^--loaded forms of hAE1 is observed for all different scenarios. However, the maximum change in the percentage of outward-facing forms in Cl^- versus citrate is only ~8%. Thus, the substantial increase in intermonomer energy transfer efficiency (corresponding to 7 Å closer distance) observed in chloride versus citrate is clearly interpretable to be due to conformational changes in hAE1 caused by chloride binding to the transport site.

When conformational distributions are compared in HCO_3^- versus citrate, a large increase is again observed in the HCO_3^--loaded forms (82−91%). Hence, the 10.6 Å closer intermonomer distance when HCO_3^- replaces citrate could again be caused by substrate anion binding. However, in the case of HCO_3^-, there is also a reorientation of the sites to the outward-facing conformation (between 20 and 70% increase). Thus, the larger change in distance with HCO_3^- replacing citrate could represent a combination of conformational changes in hAE1 caused by the binding of HCO_3^- rather than Cl^- at the substrate binding site as well as the reorientation of the transport site to the outward-facing form.

The idea that the bicarbonate-loaded outward-facing form of hAE1 has a higher energy transfer, corresponding to a shorter distance between diTBA and the FM bound to the adjacent monomer, is also consistent with the data in Figure 9B. The larger slope at the end of the debinding process (at low *x*-values) than at the beginning (high *x*-values) suggests that the energy transfer to the slowly debinding form is greater than that of the rapidly debinding form. In all cases (Table 2), the majority conformation is likely to be the EB_o form, which probably has a very slow debinding rate because the debinding rate for diTBA is very slow in bicarbonate media. In all scenarios shown in Table 2, the other major forms of hAE1 are those without bound substrates, which, from data in citrate (Figure 7C), are likely to have a faster debinding rate. Thus the data in Figure 9B is consistent with the idea that the bicarbonate-loaded forms have higher energy transfer efficiencies, and, thus, a shorter distance to FM than do the unloaded forms, a result that agrees well with the data in Table 1.

In summary, our data, particularly the decrease in FM−diTBA intermonomer distance when citrate is replaced by Cl^-, indicate that there is a significant conformational change in hAE1 caused by substrate binding. This represents the first direct physical evidence that substrate binding affects hAE1 conformation, a key element in causing the one-for-one coupling of anion exchange by facilitating the inward to outward conformational change when substrates are bound.

Further investigation of the specific parts of hAE1 involved, using site-directed mutagenesis and fluorescence labeling, should lead to a better understanding of these substantial and functionally important structural changes.

Identity of the Regions Undergoing Conformational Changes. Although the data clearly reveals conformational changes in hAE1 that are induced by substrate binding and possibly also by inside-out reorientation, the exact location of the conformationally sensitive regions cannot be specified. Because energy transfer is being observed between two different sites on the hAE1 monomer, the measured change in distance could be due to movements of both sites or to the movement of a single site.

The labeling site of FM is most likely to be at Lys-430 (*33*), which, from topology models and the nearby presence of two natural mutations (E429D and R432W) that give rise to antibodies against intact red blood cells (*41*), appears to lie in an extracellular loop (EC1) very close to the membrane surface (Figure 4B). NMR experiments indicate that labeling at the same position by EM does not prevent chloride binding to the protein but does inhibit anion transport (*42*). Therefore, labeling at this site by FM or EM probably inhibits anion exchange by preventing one or more of the conformational changes during the reaction cycle. Thus, it is unlikely that the monomer labeled by FM will undergo an inward−outward reorientation. However, the fact that the NSET efficiency is lower in absence of a transportable anion (citrate) as compared to when a substrate anion is present (Table 1) indicates that this region might be undergoing a conformational change related to anion binding (although the possibility of a difference in the amount or location of the nonspecifically bound diTBA cannot be ruled out).

Even though the exact location of diTBA binding is not known, evidence with oxonols of similar structure (*21*) strongly indicates that it interacts with a part of the protein that undergoes transport-related conformational changes. Moreover, from Figure 8, it is apparent that the diTBA off rates are much lower in bicarbonate buffers as compared to those in chloride or citrate, indicating that the diTBA binding kinetics is affected when the protein is recruited to different conformational states. Thus the observed changes in energy transfer efficiency with different anions present probably involve the movement of the diTBA binding site as well.

In conclusion, the binding of Cl^- or HCO_3^- causes a significant change in energy transfer between FM, probably bound to Lys-430 in one hAE1 monomer, and diTBA bound to the adjacent monomer. On the basis of the assumption of random orientation of the fluorophores, the energy transfer would indicate an ∼7−10 Å decrease in the distance between FM and the diTBA binding site. Alternately, part or all of the change in energy transfer could reflect a major conformational reorientation of diTBA. In either case, the data provides evidence for a substantial conformational change in hAE1. The concept of a large-scale conformational change is supported by other biochemical and biophysical evidence. For example, the binding sites for disulfonic stilbene inhibitors have been shown to be at least 15 Å away from the Glu-681 (*43*) residue, the site of proton binding during H^+−SO_4^{2-} cotransport mediated by hAE1 (*44*), which has also been implicated as part of the permeability barrier for anions (*45*). Recent data show that after the chemical modification of Glu-681 there is evidence for a second Cl^- binding site on the same hAE1 monomer as the transport site for monovalent anion exchange (*46*). Our observations also fit well with recent high-resolution crystal structures of the bacterial anion exchanger, GlpT (*47*), and the mitochondrial ATP−ADP (*48*) exchanger, which suggest a gated cavity mechanism that requires large conformational changes involving disparate parts of the protein. In particular, the substantial decrease in the apparent FM−diTBA distance when Cl^- replaces citrate agrees with models based on the crystal structure of GlpT (*47*), where it has been proposed that the protein assumes a more compact conformation upon substrate binding.

ACKNOWLEDGMENT

We acknowledge the technical assistance of Brian Holmberg in some of the steady state fluorescence measurements and Steve Atherton and Dr. Joseph Dinnocenzo for help in determining the fluorescence lifetimes by TCSPC at the Center for Photoinduced Charge Transfer, Department of Chemistry, University of Rochester.

APPENDIX 1

Expected Results for Figure 9 If there Is Only a Single Population of Specifically Bound diTBA or Two Different Subpopulations. As noted in the Discussion, under most conditions, the hAE1 molecules to which diTBA is bound will not all be in the same conformation. This gives rise to the possibility that these different diTBA populations may have different energy transfer characteristics arising, for example, because the diTBA may be located at different distances from the FM donor for the different hAE1 conformations. If these populations also have different rates of debinding from hAE1, then such heterogeneity might be manifested in the relative changes in FM and diTBA fluorescence after the addition of DIDS.

As a simple case to evaluate the possible effects of such heterogeneity, let us suppose that there are two populations of hAE1-bound diTBA, T1 and T2, characterized by different rates of debinding from hAE1. Correspondingly, when the binding of diTBA is complete, there are two populations of FM: F1 defined as FM bound to hAE1 monomers whose adjacent monomer is T1-bound and F2 with T2 bound to the adjacent monomer. There may also be a third population without any diTBA on the adjacent monomer, but this population will not exhibit any change in quenching as diTBA binding changes.

We wish to calculate the change in FM fluorescence relative to the change in diTBA fluorescence as diTBA debinds from hAE1 after the addition of DIDS, both at the beginning and at the end of the debinding process. If we assume that T1 debinds much faster than T2, then at $t \approx 0$,

$$\Delta T \approx \Delta T1 \qquad \text{(A1.1)}$$

where ΔT is the amount of diTBA released from hAE1 upon the addition of DIDS, and $\Delta T1$ is the decrease in the amount of the T1 population of diTBA. If the amount of bound diTBA decreases, as it does after DIDS addition, $\Delta T > 0$.

The change in the fluorescence emission at the FM wavelength, ΔI_F, due to this initial release of diTBA results from the conversion of some of the diTBA-quenched F1 to unquenched F1. This can be expressed as

$$\Delta I_F = \Delta I_{F1} = \frac{\gamma_F k_f \Delta T}{G} - \frac{\gamma_F k_f \Delta T}{G + k_{1T}} = \frac{\gamma_F k_f \Delta T k_{1T}}{G(G + k_{1T})} \quad (A1.2)$$

where γ_F includes the intensity of the exciting light and the extinction coefficient for FM together with any instrumental factors influencing the efficiency of detection of FM fluorescence, k_f is the radiative decay rate of the FM excited state, k_{1T} is the rate of energy transfer from the F1 population to diTBA bound to the adjacent monomer, and $G = k_f + k_{nr} + k_{ns}$, the sum of the radiative and nonradiative decay rates for FM together with the rate of energy transfer to nonspecifically bound diTBA (k_{ns}).

In the case where excitation is at 435 nm, the corresponding change in diTBA fluorescence emission, ΔI_T, at $t \approx 0$ is given by

$$\Delta I_T = \Delta I_{T1} = -\frac{\gamma_{FT} k_{1T} Q_1 \Delta T}{G + k_{1T}} \quad (A1.3)$$

where γ_{FT} is a factor that includes the intensity of the exciting light, the absorption of light by FM, and the instrumental factors that determine the efficiency of detection of fluorescence at the diTBA wavelength, Q_1 is the quantum yield of diTBA for population T1, and the other symbols are as defined in eq A1.2. Taking the quotient of A1.2 and A1.3, we obtain the change in FM fluorescence per change in diTBA fluorescence, the slope of the plots such as Figure 9A, C, and D at high diTBA fluorescence and low FM fluorescence (conditions corresponding to $t \approx 0$ after the addition of DIDS)

$$\left.\frac{\Delta I_F}{\Delta I_T}\right|_{t \approx 0} = -\frac{\gamma_F k_f}{G \gamma_{FT} Q_1} \quad (A1.4)$$

Near the end of the diTBA debinding process, when $t \to \infty$, most of the T1 population will be gone; therefore

$$\Delta T \approx \Delta T2 \quad (A1.5)$$

The change in FM fluorescence is given by an expression similar to A1.2

$$\Delta I_F = \Delta I_{F2} = \frac{\gamma_F k_f \Delta T}{G} - \frac{\gamma_F k_f \Delta T}{G + k_{2T}} = \frac{\gamma_F k_f \Delta T k_{2T}}{G(G + k_{2T})} \quad (A1.6)$$

where k_{2T} is the rate of energy transfer from FM to diTBA for population 2. The corresponding change in diTBA emission intensity for $t \to \infty$ is

$$\Delta I_T = \Delta I_{T2} = -\frac{\gamma_{FT} k_{2T} Q_2 \Delta T}{G + k_{2T}} \quad (A1.7)$$

The slope of the plot of FM fluorescence versus diTBA fluorescence after DIDS as $t \to \infty$ (high FM and low diTBA fluorescence in Figure 9) is given by the quotient of eqs A1.6 and 1.7

$$\left.\frac{\Delta I_F}{\Delta I_T}\right|_{t \to \infty} = -\frac{\gamma_F k_f}{G \gamma_{FT} Q_2} \quad (A1.8)$$

The ratio of the slope at the end of debinding to that at the beginning is given by the quotient of eqs A1.8 and A1.4

$$\frac{(\Delta I_F/\Delta I_T)_{t \to \infty}}{(\Delta I_F/\Delta I_T)_{t \approx 0}} = \frac{Q_1}{Q_2} \quad (A1.9)$$

Therefore, the slopes at the beginning and end of the diTBA debinding process are identical, as long as the quantum yields of diTBA for the two populations are the same.

In the case where diTBA is directly excited at 430 nm, as in Figure 9B, instead of being excited by the energy transfer from FM, the expressions for ΔI_F are identical to those above. However, for short times after DIDS addition, $t \approx 0$, the change in diTBA fluorescence becomes

$$\Delta I_T = \Delta I_{T1} = -\gamma_T \epsilon_1 Q_1 \Delta T \quad (A1.10)$$

where γ_T includes the intensity of the exciting light at 430 nm as well as instrumental factors that affect the efficiency of the collection of diTBA fluorescence, ϵ_1 is the extinction coefficient for the diTBA in population 1, and Q_1 is its quantum yield. Similarly, for the very last part of the diTBA debinding process after DIDS, that is, for $t \to \infty$

$$\Delta I_T = \Delta I_{T2} = -\gamma_T \epsilon_2 Q_2 \Delta T \quad (A1.11)$$

where ϵ_2 and Q_2 refer to the second, more slowly debinding population of diTBA.

Thus, the ratio of the change in FM fluorescence to the change in diTBA fluorescence at $t \approx 0$ is given by eq A1.3 divided by eq A1.10

$$\left.\frac{\Delta I_F}{\Delta I_T}\right|_{t \approx 0} = -\frac{\gamma_F k_f k_{1T}}{\gamma_T \epsilon_1 Q_1 G(G + k_{1T})} \quad (A1.12)$$

and the corresponding slope at $t \to \infty$ is given by dividing eq A1.6 by eq A1.11

$$\left.\frac{\Delta I_F}{\Delta I_T}\right|_{t \to \infty} = -\frac{\gamma_F k_f k_{2T}}{\gamma_T \epsilon_2 Q_2 G(G + k_{2T})} \quad (A1.13)$$

Therefore, the ratio of the slope at $t \to \infty$ to that at $t \approx 0$ is given by the quotient of A1.13 and A1.12

$$\frac{(\Delta I_F/\Delta I_T)_{t \to \infty}}{(\Delta I_F/\Delta I_T)_{t \approx 0}} = \frac{k_{2T} \epsilon_1 Q_1 (G + k_{1T})}{k_{1T} \epsilon_2 Q_2 (G + k_{2T})} \quad (A1.14)$$

Once again for a single population ($\epsilon_1 = \epsilon_2$, $Q_1 = Q_2$, $k_{1T} = k_{2T}$), the slopes must be the same. In this case, however, the slopes can be different even if $Q_1 = Q_2$, that is, even if the slopes for the case where all excitation is at 435 nm are the same. The most likely explanation for a difference in the slopes is probably that the two populations differ in terms of the rates of energy transfer from FM to diTBA, indicated by the terms k_{1T} and k_{2T}.

APPENDIX 2

Determination of Fractional Occupancy of hAE1 by Specifically Bound diTBA. To determine the apparent dissociation constant for specific (DIDS-sensitive) diTBA binding to hAE1, we need to factor in the depletion of the available pool of free diTBA through both specific and nonspecific binding. The following treatment parallels that of Macara and Cantley (*49*) for binding under conditions of the depletion of the ligand but in addition provides a means for determining affinity from measurements of fluorescence, rather than binding. For the overall reaction

$$T + A \overset{K_d}{\leftrightarrow} AT$$

we have

$$K_d = \frac{[T][A]}{[AT]} \Rightarrow [AT] = \frac{[T][A]}{K_d} \qquad \text{(A2.1)}$$

where $[T]$ = free diTBA, $[A]$ = free hAE1, and $[AT]$ = diTBA bound specifically to hAE1. If we define the total diTBA as T_t, the total hAE1 as A_t, and the nonspecifically bound diTBA as T_n

$$[T_t] = [T] + [AT] + [T_n] \qquad \text{(A2.2)}$$

$[T_n]$ is assumed to be proportional to the free diTBA and

$$[A_t] = [A] + [AT] \qquad \text{(A2.3)}$$

the total amount of ghost membrane (and, hence, A_t, assuming equal amounts of hAE1 per red blood cell). Thus, $[T_n] = k[T][A_t]$, where k is a proportionality constant. Hence, from equation A2.2

$$[T] = \frac{[T]_t - [AT]}{1 + k[A_t]} \qquad \text{(A2.4)}$$

From eqs (A2.1), (A2.3), and (A2.4)

$$[AT] = \frac{([T_t] - [AT])([A_t] - [AT])}{(1 + k[A_t])K_d} \qquad \text{(A2.5)}$$

$$\Rightarrow [AT]^2 - ([T_t] + [A_t] + K'_d)[AT] + [A_t][T_t] = 0 \qquad \text{(A2.6)}$$

where we define $K'_d = K_d(1 + k[A_t])$ as an apparent dissociation constant that depends on the total amount of hAE1 protein (and, thus, the total amount of red cell ghosts) present. Because we make all our measurements with 20 nM hAE1 (and correspondingly, the same amount of binding capacities of the nonspecific sites), K'_d is a useful empirical parameter. We can solve the quadratic eq A2.6 to obtain

$$[AT] = \frac{[T_t] + [A_t] + K'_d - \sqrt{([T_t]^2 - 2[T_t][A_t] + 2[T_t]K'_d + 2[A_t][K'_d] + [A_t]^2 + K'^2_d)}}{2} \qquad \text{(A2.7)}$$

Because we measure fluorescence, rather than actual amounts of the various species of diTBA, it is useful to introduce an equation for total fluorescence F_T

$$F_T = f_s[AT] + f_{ns}[T_n] + f_{free}[T] \qquad \text{(A2.8)}$$

where f_s, f_{ns}, and f_{free} are constants that include extinction coefficients, instrument constants, and quantum yields for the respective forms of diTBA. Using eq A2.4 and $[T_n] = k[T][A_t]$ eq A2.8 can be rewritten as

$$F_T = f_s[AT] + (f_{ns}k[A_t] + f_{free})\frac{[T_t] - [AT]}{1 + k[A_t]} \qquad \text{(A2.9)}$$

and after some further rearrangement as

$$F_T = \left(f_s - \frac{f_{ns}k[A_t] + f_{free}}{1 + k[A_t]}\right)[AT] + \frac{[T_t](f_{ns}k[A_t] + f_{free})}{1 + k[A_t]} \qquad \text{(A2.10)}$$

After measuring the fluorescence intensities of the different amounts of diTBA ($[T_t]$) in the presence of ghosts (20 nM hAE1), we added DIDS to remove the specifically bound diTBA, reducing $[AT]$ to zero. Subtracting the fluorescence intensities before and after DIDS addition gives a measure of the fluorescence due to $[AT]$. If $F_{diTBA-DIDS}$ is the value of this fluorescence intensity

$$F_{diTBA-DIDS} = F_T - F_{DIDS} = \left(f_s - \frac{f_{ns}k[A_t] + f_{free}}{1 + k[A_t]}\right)[AT] \qquad \text{(A2.11)}$$

Substituting eq A2.7 for $[AT]$

$$F_{diTBA-DIDS} = F \cdot \frac{[T_t] + [A_t] + K'_d - \sqrt{([T_t]^2 - 2[T_t][A_t] + 2[T_t]K'_d + 2[A_t][K'_d] + [A_t]^2 + K'^2_d)}}{2} \qquad \text{(A2.12)}$$

where F is a constant with respect to $[AT]$ and $[T_t]$, is defined according to eq A2.11 as

$$F = f_s - \frac{f_{ns}k[A_t] + f_{free}}{1 + k[A_t]} \qquad \text{(A2.13)}$$

The data obtained by plotting $F_{diTBA-DIDS}$ versus $[T_t]$ in the different buffers was fitted to eq A2.12 using Origin 7.0 to obtain the respective K'_d values. For the energy transfer experiments in each buffer, the respective K'_d value is inserted into eq A2.7 to obtain $[A_t]_{[T_t]=x}$, the amount of diTBA bound to hAE1 when a particular amount of diTBA is added. For this calculation, the value of $[A_t]$ is taken as $[A_t]' = (1 - p)20$ nM, where p is the fractional inhibition of Cl^- exchange by FM. This is done because diTBA cannot bind to the hAE1 monomers that are already labeled by FM. It does not, however, invalidate our assumption for determining K'_d, however, because the total amount of ghosts added remains the same. The fractional occupation f is obtained as $f = [AT]_{[T_t]=x}/[A_t]'$.

REFERENCES

1. Knauf, P. A., and Pal, P. (2003) in *Red Cell Membrane Transport in Health and Disease* (Bernhardt, I., and Ellory, J. C., Eds.) pp 253−301, Springer, Berlin.
2. Low, P. S. (1986) Structure and function of the cytoplasmic domain of band 3: center of erythrocyte membrane-peripheral protein interactions, *Biochim. Biophys. Acta 864*, 145−167.

3. Zhang, D., Kiyatkin, A., Bolin, J. T., and Low, P. S. (2000) Crystallographic structure and functional interpretation of the cytoplasmic domain of erythrocyte membrane band 3, *Blood 96*, 2925−2933.
4. Wang, D. N., Sarabia, V. E., Reithmeier, R. A. F., and Kuhlbrandt, W. (1994) Three-dimensional map of the dimeric membrane domain of the human erythrocyte anion exchanger, band 3, *EMBO J. 13*, 3230−3235.
5. Wang, D. N., Kuhlbrandt, W., Sarabia, V. E., and Reithmeier, R. A. F. (1993) Two-dimensional structure of the membrane domain of human band 3, the anion transport protein the erythrocyte membrane, *EMBO J. 12*, 2233−2239.
6. Casey, J. R., and Reithmeier, R. A. F. (1991) Analysis of the oligomeric state of band 3, the anion transport protein of the human erythrocyte membrane, by size exclusion high performance liquid chromatography. Oligomeric stability and origin of hetrogeneity, *J. Biol. Chem. 266*, 15726−15737.
7. Jennings, M. L. (1984) Oligomeric structure and the anion transport function of human erythrocyte band 3 protein, *J. Membr. Biol. 80*, 105−117.
8. Steck, T. L. (1972) Cross-linking the major proteins of the isolated erythrocyte membrane, *J. Mol. Biol. 66*, 295−305.
9. Blackman, S. M., Piston, D. W., and Beth, A. H. (1998) Oligomeric state of human erythrocyte band 3 measured by fluorescence resonance energy homotransfer, *Biophys. J. 75*, 1117−1130.
10. Macara, I. G., and Cantley, L. C. (1981) Mechanism of anion exchange across the red cell membrane by band 3: interactions between stilbenedisulfonate and NAP-taurine binding sites, *Biochemistry 20*, 5695−5701.
11. Fujinaga, J., Tang, X.-B., and Casey, J. R. (1999) Topology of the membrane domain of human erythrocyte anion exchange protein, AE1, *J. Biol. Chem. 274*, 6626−6633.
12. Tang, X.-B., Fujinaga, J., Kopito, R., and Casey, J. R. (1998) Topology of the region surrounding Glu^{681} of human AE1 protein, the erythrocyte anion exchanger, *J. Biol. Chem. 273*, 22545−22553.
13. Zhu, Q., Lee, D. W., and Casey, J. R. (2003) Novel topology in C-terminal region of the human plasma membrane anion exchanger, AE1, *J. Biol. Chem. 278*, 3112−3120.
14. Popov, M., Tam, L. Y., Li, J., and Reithmeier, R. A. F. (1997) Mapping the ends of transmembrane segments in a polytopic membrane protein. Scanning N-glycosylation mutagenesis of extracytosolic loops in the anion exchanger, band 3, *J. Biol. Chem. 272*, 18325−18332.
15. Popov, M., Li, J., and Reithmeier, R. A. F. (1999) Transmembrane folding of the human erythrocyte anion exchanger (AE1, band 3) determined by scanning and insertional N-glycosylation mutagenesis, *Biochem. J. 339*, 269−279.
16. Fröhlich, O., Leibson, C., and Gunn, R. B. (1983) Chloride net efflux from intact erythrocytes under slippage conditions. Evidence for a positive charge on the anion binding/transport site, *J. Gen. Physiol. 81*, 127−152.
17. Knauf, P. A., Fuhrmann, G. F., Rothstein, S., and Rothstein, A. (1977) The relationship between anion exchange and net anion flow across the human red blood cell membrane, *J. Gen. Physiol. 60*, 363−386.
18. Knauf, P. A., Law, F.-Y., and Marchant, P. J. (1983) Relationship of net chloride flow across the human erythrocyte membrane to the anion exchange mechanism, *J. Gen. Physiol. 81*, 95−125.
19. Knauf, P. A., and Brahm, J. (1989) in *Methods in Enzymology*, (Fleischer, S. and Fleischer, B., Eds.) Vol. 173, pp 432−453, Academic Press, New York.
20. Liu, D., Kennedy, S. D., and Knauf, P. A. (1996) Source of transport site asymmetry in the band 3 anion exchange protein determined by NMR measurements of external Cl^- affinity, *Biochemistry 35*, 15228−15235.
21. Knauf, P. A., Raha, N. M., and Spinelli, L. J. (2000) The noncompetitive inhibitor WW781 senses changes in erythrocyte anion exchanger (AE1) transport site conformation and substrate binding, *J. Gen. Physiol. 115*, 159−173.
22. Knauf, P. A., Law, F. Y., Leung, T. W., Gehret, A. U., and Perez, M. L. (2002) Substrate-dependent reversal of anion transport site orientation in the human red blood cell anion-exchange protein, AE1, *Proc. Natl. Acad. Sci. U.S.A. 99*, 10861−10864.
23. Knauf, P. A. (2002) in *Membrane Transport and Renal Physiology, IMA Volumes in Mathematics and its Applications* (Layton, H. E. and Weinstein, A. M., Eds.) Vol. 129, pp 85−100, Springer, New York.
24. Wieth, J. O., and Brahm, J. (1980) in *Membrane Transport in Erythrocytes* (Lassen, U. V., Ussing, H. H., and Wieth, J. O., Eds.) pp 467−482, Munksgaard, Copenhagen, Denmark.
25. Selvin, P. R. (1995) Fluorescence resonance energy transfer, *Methods Enzymol. 246*, 300−334.
26. Pal, P., and Knauf, P. A. (2002) Substrates induce conformational changes in human red cell anion exchanger 1 (AE1) as observed by FRET, *Biophys J. 82*, 553a.
27. Dalmark, M., and Wieth, J. O. (1972) Temperature dependence of chloride, bromide, iodide, thiocyanate and salicylate transport in human red cells, *J. Physiol. 224*, 583−610.
28. Steck, T. L. (1974) The organization of proteins in the human red blood cell membrane: a review, *J. Cell Biol. 62*, 1−19.
29. Lebedev, D. V. (2000) Role of volume-sensitive anion and amino acid fluxes in regulatory volume decrease in HL-60 cells and fluorescence energy transfer studies of the human band 3 anion exchange protein after fluorescein malemide labeling, University of Rochester, Rochester, NY.
30. Rao, A., Martin, P., Reithmeier, R. A. F., and Cantley, L. C. (1979) Location of the stilbene disulfonate binding site of the human erythrocyte anion-exchange system by resonance energy transfer, *Biochemistry 18*, 4505−4516.
31. Griep, M. A., and McHenry, C. S. (1990) Dissociation of the DNA polymerase III holoenzyme beta 2 subunits is accompanied by conformational change at distal cysteines 333, *J. Biol. Chem. 265*, 20356−20363.
32. Schopfer, L. M., and Salhany, J. M. (1998) Spectroscopic and kinetic characterization of eosin-5-maleimide, *Anal. Biochem. 257*, 139−148.
33. Bicknese, S., Rossi, M., Thevenin, B. J., Shohet, S. B., and Verkman, A. S. (1995) Anisotropy decay measurement of segmental dynamics of the anion binding domain in erythrocyte band 3, *Biochemistry 34*, 10645−10651.
34. Cobb, C. E., Lin, H., and Beth, A. H. (1990) Identification of the eosin-5-maleimide and eosin-5-iodoacetamide reaction sites on human erythrocyte band 3, *Biophys. J. 57*, 96a.
35. Cobb, C. E., and Beth, A. H. (1990) Identification of the eosinyl-5-maleimide reaction site on the human erythrocyte anion-exchange protein: overlap with the reaction sites of other chemical probes, *Biochemistry 29*, 8283−8290.
36. Rao, A., and Reithmeier, R. A. F. (1979) Reactive sulfhydryl groups of the band 3 polypeptide from human erythrocyte membranes, *J. Biol. Chem. 254*, 6144−6150.
37. Pratap, P. R., Novak, T. S., and Freedman, J. C. (1990) Two mechanisms by which fluorescent oxonols indicate membrane potential in human red blood cells, *Biophys. J. 57*, 835−849.
38. Knauf, P. A. (2000) Effects of temperature and chemical modification of GLU-681 on kinetics of binding of a fluorescent oxonol dye to AE1 (band 3), *Biophys. J. 78*, 257A.
39. Knauf, P. A., Gasbjerg, P. K., and Brahm, J. (1996) The asymmetry of chloride transport at 38 °C in human red blood cell membranes, *J. Gen. Physiol. 108*, 577−589.
40. Liu, S. J., Law, F.-Y., and Knauf, P. A. (1996) Effects of external pH on substrate binding and on the inward chloride translocation rate constant of band 3, *J. Gen. Physiol. 107*, 271−291.
41. Jarolim, P., Rubin, H. L., Zakova, D., Storry, J., and Reid, M. E. (1998) Characterization of seven low incidence blood group antigens carried by erythrocyte band 3 protein, *Blood 92*, 4836−4843.
42. Liu, D., Kennedy, S. D., and Knauf, P. A. (1995) ^{35}Cl nuclear magnetic resonance line broadening shows that eosin-5-maleimide does not block the external anion access channel of band 3, *Biophys. J. 69*, 399−408.
43. Knauf, P. A., Law, F. Y., Leung, T. W., and Atherton, S. J. (2004) Relocation of the disulfonic stilbene sites of AE1 (band 3) on the basis of fluorescence energy transfer measurements, *Biochemistry 43*, 11917−11931.
44. Jennings, M. L., and Smith, J. S. (1992) Anion-proton cotransport through the human red blood cell band 3 protein: role of glutamate 681, *J. Biol. Chem. 267*, 13964−13971.
45. Tang, X.-B., Kovacs, M., Sterling, D., and Casey, J. R. (1999) Identification of residues lining the translocation pore of human AE1, plasma membrane anion exchange protein, *J. Biol. Chem. 274*, 3557−3564.

46. Jennings, M. L. (2005) Evidence for a second binding/transport site for chloride in erythrocyte anion transporter AE1 modified at glutamate 681, *Biophys J. 88*, 2681−2691.
47. Huang, Y., Lemieux, M. J., Song, J., Auer, M., and Wang, D. N. (2003) Structure and mechanism of the glycerol-3-phosphate transporter from *Escherichia coli*, *Science 301*, 616−620.
48. Pebay-Peyroula, E., Dahout-Gonzalez, C., Kahn, R., Trezeguet, V., Lauquin, G. J., and Brandolin, G. (2003) Structure of mitochondrial ADP/ATP carrier in complex with carboxyatractyloside, *Nature 426*, 39−44.
49. Macara, I. G., and Cantley, L. C. (1981) Interactions between transport inhibitors at the anion binding sites of the band 3 dimer, *Biochemistry 20*, 5095−5105.

BI051916R